Christoph Grimmer

Activity and Stability Enhancement of Platinum Cobalt Catalysts for HTPEM Fuel Cells

MASTER THESIS

zur Erlangung des akademischen Grades eines Diplom-Ingenieurs
der technischen Wissenschaften

erreicht an der

Technischen Universität Graz

Betreuer:

Assoc.Prof. Dipl.-Ing. Dr. Viktor Hacker

Labor für Brennstoffzellenentwicklung
Institut für Chemische Verfahrenstechnik und Umwelttechnik
Technische Universität Graz

13. Februar 2013

Statutory declaration

I declare that I have authored this thesis independently, that I have not used other than the declared sources/resources, and that I have explicitly marked all material which has been quoted either literally or by content from the used sources.

_____ Date

_____ Signature

“Innovation – ein Prozess
schöpferischer Zerstörung”
Joseph Schumpeter

meinen Eltern

Abstract

The aim of this work is the development of highly active and stable platinum-cobalt-compound catalysts for the oxygen reduction reaction in high temperature polymer electrolyte membrane (PEM) fuel cells. In cooperation with elcomax GmbH Munich, Germany we work on implementing these new catalysts in a big scale production process.

Platinum and Cobalt salts in various ratios are dissolved in an impregnation solution with reducing agents. An appropriate amount of these solutions is displaced on gas diffusion electrode layer sheets that are coated with an active layer based on high surface area carbon. By thermal treatment the precursor salts are reduced to nanocrystalline highly catalytic active particles.

Because nanoparticles tend to agglomerate and non-noble metals oxidize and dissolve in acidic conditions, long time stability of PEM fuel cells is limited. Several stabilizing procedures were developed: e.g. acid leaching steps, deposition of additional platinum layers, annealing steps and the implementation of surfactants into our production process. Together with our partner an accelerated stress test protocol was developed to characterize and compare the stability and verify the stabilizing strategies.

Kurzfassung

Das Ziel dieser Arbeit ist die Entwicklung von hochaktiven und stabilen Platin-Cobalt-Verbindungskatalysatoren für die Sauerstoffreduktionsreaktion in Hochtemperatur-polymerelektrolytbrennstoffzellen. In Kooperation mit elcomax GmbH, München wird das Ziel verfolgt, diese neuen Katalysatormaterialien in den großtechnischen Produktionsprozess einzubetten.

Platin- und Cobaltsalze in verschiedenen Verhältnissen werden mit Reduktionsmitteln in Lösung gebracht. Das entsprechende Volumen dieser Lösung wird auf eine Gasdiffusionselektrode mit einer Aktivschicht basierend auf Kohlenstoff mit hoher Oberfläche aufgebracht. Durch die Temperaturbehandlung werden die Precursorsalze zu nanokristallinen, katalytisch hochaktiven Partikeln reduziert.

Die Langzeitstabilität von Brennstoffzellen wird durch die Agglomeration der Nanopartikel und die Oxidation der unedlen Metalle im sauren Milieu beeinflusst. Um die Stabilität der Katalysatoren zu erhöhen wurden Stabilisierungsverfahren wie z.B. Säure-Leaching Schritte, Abscheidung einer zusätzlichen Platinschicht, Tempern der Katalysatoren und Stabilisierung durch Tenside entwickelt. Mit dem Kooperationspartner wurde ein Protokoll für beschleunigte Stresstests entwickelt um die Stabilität zu charakterisieren und zu vergleichen und um die Stabilisierungsmaßnahmen zu verifizieren.

Acknowledgements – Danksagung

In erster Linie möchte ich meinen Eltern danken, die durch großzügigste finanzielle und vor allem persönliche und moralischen Unterstützung mein Studium ermöglicht haben. Vielen Dank!

Weiterer großer Dank gilt all meinen Freunden, die mich durch mein Studium begleitet haben und diese Zeit zu einer ganz Besonderen machten. Aus diesem Kreis möchte ich besonders meine Freundin Dani und meine Schwester Lena betonen.

Besonderer Dank gilt auch Assoc.-Prof. Dipl.-Ing. Dr. Viktor Hacker sowie Mag. Markus Perchthaler für die Möglichkeit diese Arbeit zu verfassen und die wissenschaftliche Begleitung während der Zeit der praktischen Laborarbeiten.

Hervorheben möchte ich bei dieser Gelegenheit meinen Betreuer Dipl.-Ing. Alexander Schenk, der mich nicht nur durch großartige fachliche Unterstützung und Kompetenz begleitet hat, sondern auch durch seine Freundschaft die gesamte Zeit meiner Arbeit bereichert hat.

Dankbarkeit gilt allen KollegInnen am Labor für Brennstoffzellensysteme, die mich durch zahlreiche Diskussionen und Ratschlägen unterstützt haben. Für die Durchführung der thermogravimetrischen Untersuchungen möchte ich mich bei Josefine Hobisch bedanken.

Ohne euch wären mein Studium und diese Arbeit nicht möglich gewesen!

Table of Contents

1 Introduction

1.1 Electricity

Widespread electrification, available and affordable for everyone, is one of the major achievements of modern civilized societies. Considering ever-growing economies and rising demand for energy on the one hand and depleting fossil resources on the other hand, it is one of the big challenges of the 21st century to ensure electric power generation and stable networks.

Key factors for this challenge are the use of renewable primary energy sources and highly efficient technologies for energy generation, storage and consumption. Mixtures of various technologies that meet the criteria of using renewable resources are already available. Concerning most of these technologies e.g. photovoltaics and wind powered electricity generation, there is the need to overcome their fluctuation of power generation due to dependence on weather conditions. To face this difficulty one can think of two solutions, first to install energy storage devices and second to increase the share of non-fluctuant sources. Fuel Cells, especially in stationary applications could be a key technology to solve the second requirement. To be compatible with conventional technologies that are operated with fossil resources, costs of fuel cells have to be further reduced. Since big parts of the costs are due to the use of platinum as catalyst the development of new catalysts plays an important role for the commercialization of this promising and pioneering technology.

1.2 Fuel Cells

Fuel cells (tertiary cells) are electrochemical cells that convert chemical energy directly in electric energy in a highly efficient way. Hydrogen, syngas and methanol are the most widely used fuels that are oxidized to water and carbon dioxide respectively. As oxidant pure oxygen or air is used.

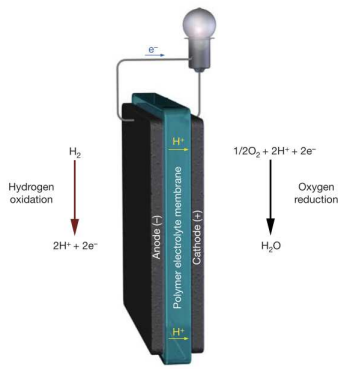

Figure 1: Scheme of a Polymer Electrolyte Membrane (PEM) Fuel Cell [1]

Fuel cells can be distinguished by the charge transport species, operating temperature, electrolyte or fuel.

Charge transport:

- Acidic FCs — Charge transport by protons
- Basic FCs — Charge transport by hydroxide ions
- Molten carbonate FCs — Charge transport by carbonate
- Solid oxide FCs — Charge transport by oxygen anions

Operating temperature:

- Low Temperature FCs — below 100°C
- Medium Temperature FCs — between 100 and 250°C
- High Temperature FCs — above 400°C

Electrolyte

- Liquid — typically aqueous solutions
- Solid — typically polymers or ceramics

Fuel:

- Hydrogen
- Methanol (or Ethanol)
- Syngas (by steam reforming)

Different kinds of fuel cells are optimally used for different applications. The LT-PEMFC is a potential candidate for mobile applications while the HT-PEMFC is primary used in stationary applications. For portable applications the direct methanol fuel cell is a promising candidate that is also commercially available. HT-FCs that are operated above 400°C like the SOFC are technologies for big scale stationary applications.

1.3 Polymer Electrolyte Membrane Fuel Cells (PEMFCs)

1.3.1 General aspects

The PEMFC uses hydrogen as fuel and an acidic proton-conducting polymer as membrane. The cell reaction is and its thermodynamics are [2]:

$$H_2 + ½\ O_2 \rightarrow H_2O$$

ΔH = - 285.5 kJ/mol (= 1.48 V)

ΔS = - 163.5 J/K/mol (below 100°C)

ΔS = - 44.5 J/K/mol (above 100°C)

The theoretical potential of a hydrogen fuel cell at 25°C is therefore 1.229 V.

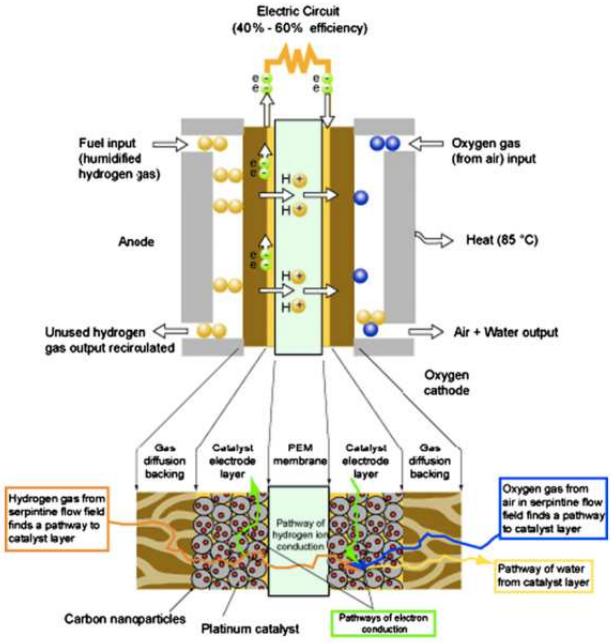

Figure 2: Scheme of a PEM-FC [3]

There are still some technological aspects that have to be solved before PEMFCs can penetrate the market. One key aspect is the development of highly active, low cost and most importantly stable catalysts. State of the art catalysts for PEMFCs consist of pure platinum and are therefore responsible for approximately 30 % of the manufacturing costs [4].

In this work catalysts for High Temperature Polymer Electrolyte Fuel Cells are developed. High temperature means 160-200°C in this respect.

1.3.2 Membranes

Membranes for PEMFCs have to be good proton conductors, chemical, thermal and mechanical stable, an electrical isolator and not permeable for hydrogen. They are usually quite thin (~ 10 – 100 µm) and have a high influence on the cell performance because they are responsible for the current transport (in form of protons) [3].

The standard membrane for LT-PEMs is a perfluorosulfonic acid (PFSA) based polymer such as Nafion®. It consists of a polytetrafluoroethylene backbone (like Teflon®) that gives the membrane physical and chemical stability and sulfonic acid groups that are responsible for the proton conductivity [3].

Since sulfonated polymers need to be humidified for proton conductivity they do not meet this criterion in temperature regimes above 100°C. For HT-PEMs there are different membranes [5]:

- Modified PFSA membranes (with hydroscopic oxides)
- Sulfonated polyaromatic polymers (such as PBI, polybenzimidazole)
- Acid-base polymer membranes (such as phosphoric acid doped PBI)

1.4 Efficiency of fuel cells

In principle the efficiency is the ratio of electrical energy output to energy input. Because the energy input of hydrogen can be given in various values there is no general definition of efficiency.

The energy value of hydrogen can be given as higher heating value (ΔH^0_{HHV} = -285.6 kJ/mol, $E_{th,HHV}$ = 1.48 V) or as lower heating value (ΔH^0_{HHV} = -241.2 kJ/mol, $E_{th,HHV}$ = 1.25 V). The HHV is higher because the reaction product water is considered to be liquid. In the case of the LHV the product water is gaseous. The difference between the HHV and the LHV is the heat of vaporization [6].

Because there are also irreversible losses in form of entropy only the Gibbs free energy can be converted (ΔG^0_l = -237.4 kJ/mol, $E_{rev,l}$ = 1.23 V) to electrical energy. So the theoretically ideal efficiency can be given by

$$\eta_{id} = \frac{E_{rev}}{E_{th}}, \tag{1}$$

which gives us the value of 83 % in the case of HHV and liquid product water.

The electric efficiency of an operated fuel cell can be given by

$$\eta_{el} = \frac{E}{E_{rev}}. \tag{2}$$

The electrical efficiency of energy conversion of a PEMFC is in the range of 35 – 70 % [7].

The theoretic efficiency of a heat engine is given by the Carnot efficiency.

$$\eta_C = \frac{T_2 - T_1}{T_2} \tag{3}$$

T_1 temperature of exhaust
T_2 temperature of combustion

Fuel cells are in principle able to convert energy more efficient than Carnot limited heat engines. If the waste heat of a fuel cell is recovered an overall efficiency of over 90 % can be achieved (e.g. Elcore 2400).

1.5 High temperature PEM

The main advantages of operating a PEMFC at evaluated temperatures are [2]:

- Enhanced anode and cathode reaction kinetics
- Higher carbon monoxide (CO) tolerance
- Simpler cooling and waste heat recovery
- Simpler water management (only in gaseous phase)

1.5.1 Enhanced kinetics

Since the hydrogen oxidation reaction (HOR) is much faster (i_0 = 10^{-3} to 10^{-4} A/cm^2) than the oxygen reduction reaction (ORR) (i_0 = 10^{-8} to 10^{-9} A/cm^2) the overall kinetics is determined by the ORR. The kinetics can be described by the Tafel equation [2]:

$$E = E_{rev} + b \log i_0 - b \log i \tag{4}$$

with

$$b = -2.3 \frac{R\,T}{\alpha\, n\, F} \tag{5}$$

E	electrode potential
E_{rev}	reversible electrode potential
b	Tafel slope
i	current density
i_0	exchange current density
n	transferred electrons
α	transfer coefficient

The effect of evaluated temperatures on the Tafel slope b and the exchange current density is positive. The theoretical correlation between b and T is given by differentiating equation (5):

$$\frac{\delta b}{\delta T} = -\frac{2.3R}{\alpha nF} \quad (6)$$

So the theoretical change in b is approximately 0.2 mV/K (assuming α is not influenced by T). However, experiments showed that the Tafel slope increase with temperature only at low current densities. It seems to be constant in high current density regions. *Zhang et al.* also report that there is an increase of i_0 with an increase of temperature from 303 to 343 K of about one magnitude (there is no data in the literature about the change of i_0 above 100°C) [2].

The thermodynamic aspect of evaluated temperatures on the other hand is negative. E_{rev} depends negatively on the temperature because the entropy ΔS of the cell reaction is negative. From the equation

$$\frac{\delta E_{rev}}{\delta T} = \frac{\Delta S}{nF} \quad (7)$$

E_{rev} can be calculated and changes by -0.85 mV/K below 100°C and -0.23 mV/K above 100°C respectively. The open circuit voltage (OCV) is the voltage that can be achieved when the current is zero. Based on the theoretical cell voltages described above the OCV can be calculated by the following equation:

$$OCV = 1.23 - 0.9 * 10^{-3}(T - 298) + 2.3\frac{RT}{nF}\log\frac{p_{H2}^2 p_{O2}}{p_{H2O}} \quad (8)$$

In general it can be said that the positive effects of i_0 and b overcompensate the negative effects of thermodynamic aspects and operating a PEMFC at elevated temperatures increases the reaction rate.

1.5.2 Higher CO tolerance

For some applications it may be preferable to use hydrogen from syngas instead of pure hydrogen. Syngas from steam reforming contains a considerable amount of carbon monoxide that has a high affinity to platinum surfaces and is therefore a poison for platinum and platinum alloy catalysts. At an operating temperature of 80°C the fuel cell performance decreases at CO concentrations of only 10-20 ppm. *Yang et al.* calculated the coverage of CO on a platinum surface and plotted it against the temperature (see Figure 3) [8].

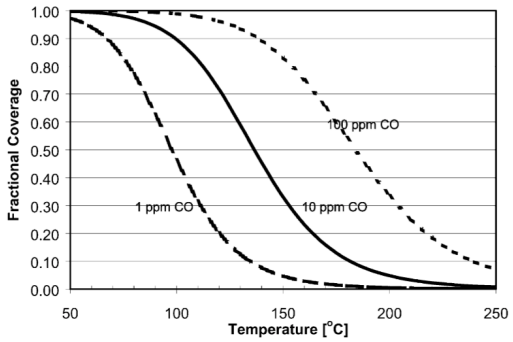

Figure 3: CO coverage of a platinum surface at different CO concentrations [8]

As illustrated above the CO tolerance is increased dramatically at higher temperatures. *Li et al.* define CO tolerance as voltage loss of less than 10 mV and find the following tolerances [9]:

- 80°C 0.0025 % (25 ppm)
- 125°C 0.1 %
- 200°C 3 %

For operating a PEMFC with syngas it is therefore necessary to either purify the hydrogen or to operate the fuel cell at temperatures close to 200°C.

1.5.3 Simpler cooling and waste heat recovery

The operation of a PEMFC at 80°C generates a lot of heat that has to be removed by any kind of cooling system. An active cooling system requires energy to remove waste heat and therefore lowers the overall efficiency. It is easier to cool a system if the temperature difference to the environment is bigger. Simplifying the cooling system and employing the waste heat for a steam gas reformer or direct heating can significantly increase the efficiency [2].

1.5.4 Simpler water management

Water management is an important issue in a PEMFC with a perfluorosulfonic acid based polymer. Too less water can dry out the membrane and leads to a loss of proton conductivity. Too much water inside the cell can cause flooding, which means that liquid water blocks gas channels. In both cases the cell performance decreases significantly.

Since there is no liquid water in a HT-PEMFC, membranes that are independent of humidification are used and enable a simplified water management. Additionally gas diffusion is much faster and allows a simpler design of flowfields.

1.5.5 Problems operating a PEMFC at evaluated temperatures

Although water management in general is simpler, dehydration of the membrane is an important issue. Degradation of components of the cell is another problem that has to be considered [2].

1.5.6 Degradation of Pt based electrocatalyst

Platinum and platinum alloy catalysts in form of nanoparticles are usually supported on carbon matrices to ensure a high electrochemical active surface area (ECSA).

In principle there are two problems concerning the catalyst:

- Particle agglomeration
- Platinum dissolution

1.5.6.1 Particle agglomeration

Platinum based nanoparticles agglomerate at higher temperatures and during the PEMFC operation (see Figure 4).

Because of two contrary aspects that have to be considered it is not trivial to determine the optimal size of the nanoparticles. These two aspects are:

- Smaller particles have a greater surface area
- Bigger particles show increased activity concerning ORR [10]

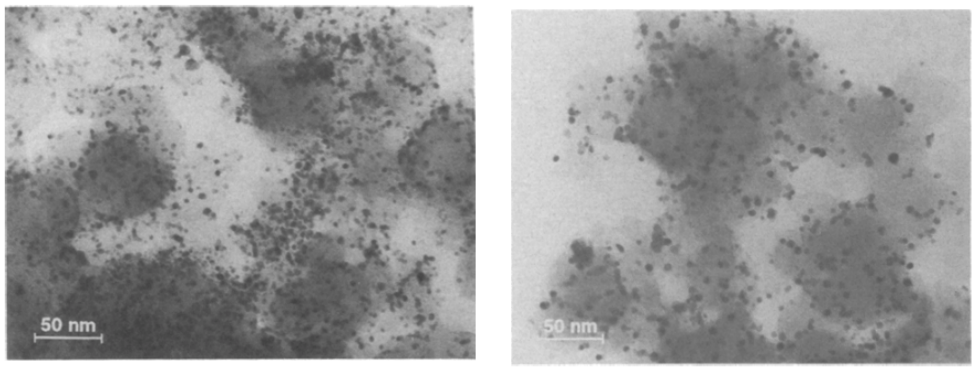

Figure 4: TEM image of cathode catalyst layer after 70 h and 2200 h operation [10]

As can be seen from Figure 4 and Figure 5 the particles grow while the cell performance is almost constant. *Wilson* explains that finding by the formation of more active surface crystal faces during agglomeration. In other words, the specific activity (mA/cm^2) increases with particle size [10,11].

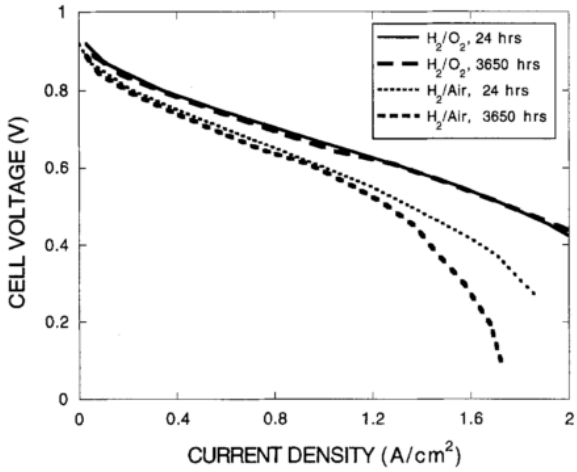

Figure 5: Polarization curve of a PEMFC at 80°C (0.50 V, anode loading: 0.14 mg Pt/cm^2, cathode loading: 0.23 mg Pt/cm^2) [10]

In agreement with *Wilson* it was found that depending on the electrolyte the specific activity is related to the crystalline surface. Pt(111) is the most active face in perchloric acid while Pt(100) is most active in sulfuric acid. This is explained by the high affinity of sulfate ions to the Pt(111) surface. In sulfuric acid the relative activity is Pt(111) < Pt(100) < Pt(110) while in perchloric acid the surface activity behaves like Pt(100) < Pt(110) < Pt(111) respectively [12–14].

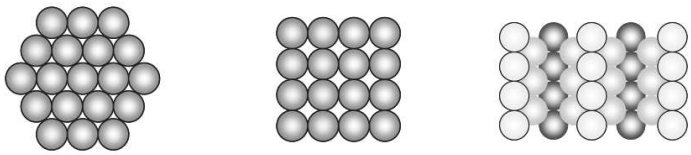

Figure 6: Crystalline structure of a) Pt(111), b) Pt(110) and c) Pt(100) [13]

It is known that the faces Pt(111) and Pt(100) occur most often in high disperse Pt/C catalysts [14].

Especially in the case of Pt-Co alloy catalysts there is an increase in activity with increasing diameter up to a certain value [15,16]. *Jayasayee et al.* investigated this phenomenon on nanoparticles between 2 and 10 nm and found that the particle size and specific activity are correlating. It also turned out that PtM (M = Co, Ni, Cu) alloys have a greater correlation than Pt/C (see Figure 7) [16].

The optimal size of a Pt nanoparticle is reported to be ~ 3 nm while in the case of Pt-Co bimetallic nanoparticles 4-5 nm [14,16,17] is reported. This is explained by less affinity of OH on larger particles due to a change in the d-band vacancy [18]. The detailed effect of Pt-Pt distance and Pt d-band vacancy on catalytic activity is explained in section 1.6.2.

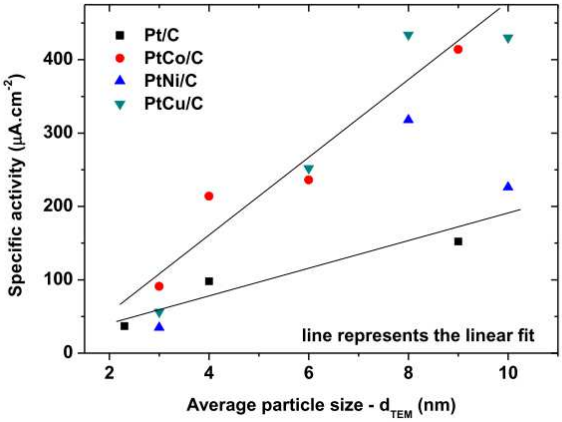

Figure 7: Correlation between particle size and specific activity [16]

1.5.6.2 Platinum dissolution

Since platinum is a noble metal (E_0 = 1.18 V) it is in principle stable under acidic conditions [19]. However, platinum nanoparticles can dissolve according to these proposed reactions [2]:

$$Pt \rightarrow Pt^{2+} + 2e^-$$

$$Pt + H_2O \rightarrow PtO + 2H^+ + 2e^-$$

$$PtO + 2H^+ \rightarrow Pt^{2+} + 2H_2O$$

1.6 Catalysts for HT-PEM FCs

A standard catalyst layer consists of the following phases:

- Carbon support with catalyst nanoparticles
- Ionomer
- Gas diffusion channels, pores

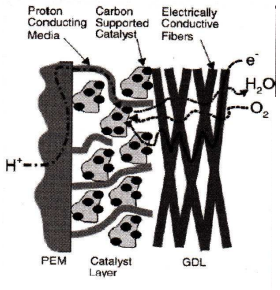

Figure 8: Scheme of an active layer between the PEM and the GDL [20]

The electrochemical reaction is only possible at sites where all three phases are present. The carbon support generates a high surface area and is the electric conductor, the ionomer conducts the protons and pores are necessary for reactant and product transport to and from the active site [3].

For HT-PEMFCs platinum is still the catalyst of choice on the anode as well as on the cathode side. In general the catalyst loading is higher on the cathode side as the HOR has a much faster kinetic than the ORR (see section 1.5.1). In the last decades much progress has been made to reduce and eventually replace platinum [13].

1.6.1 State-of-the-art platinum catalyst

Commercial available platinum catalysts are usually prepared by precipitation methods. Soluble platinum species (e.g. salts) are deposited (reduced) on a high surface support material, mainly carbon [21].

The state-of-the-art catalyst layers are produced by impregnation of the gas diffusion electrodes (GDEs) with a platinum salt solution and reduction by hydrogen gas.

1.6.2 Pt bimetallic catalysts

Due to relative high overpotentials of the ORR on platinum catalysts (approximately 400 mV at 1.5 A/cm²) and high costs of platinum, it is necessary to develop more active catalysts that lead to a reduction of the platinum loading (currently 0.5 – 1 mg Pt/cm²) [14].

One strategy of reducing the Pt loading is to enhance the activity by alloying the nanoparticles with transition metals such as Co, Ni, Cu, Fe, Cr, V, Ti or Ag [11,14]. The increased electrocatalytic activity of Pt_3M catalysts can be explained by [14]:

- Decreased Pt-Pt distance
- Inhibition of OH_{ads} formation on surface
- Roughening of the surface structure
- D-band vacancies

1.6.2.1 Decrease of Pt-Pt distance

Experiments showed that smaller transmission metal atoms substitute platinum atoms and therefore contract the lattice of the crystalline structure. Because of this contraction there is a good correlation between bond distance and electrocatalytic activity [14].

The results from *Jayasayee et al.* concerning lattice constants and specific activity are summarized in Table 1. The findings indicate that specific activity increases with decreasing lattice constants [16].

Table 1: Summarize of lattice constants and specific activity of PtM catalysts (lattice constants from XRD analysis, particle size from TEM, specific activity from ex-situ characterization by CV in O_2 saturated $HClO_4$ at 0.9 V on a rotating disk electrode RDE) [16]

	Lattice constant	Particle size	Specific activity
	Å	nm	µA/cm²
Pt/C	**3.92**	**2.3 ± 0.8**	**37**
$Pt_{81}Co_{19}/C$	**3.85**	**3 ± 1**	**91**
$Pt_{60}Ni_{40}/C$	**3.75**	**3 ± 1**	**35**
$Pt_{50}Ni_{50}/C$	**3.72**	**-**	**163**
$Pt_{81}Cu_{19}/C$	**3.86**	**3 ± 1**	**56**

1.6.2.2 Inhibition of OH_{ads} formation on surface

Stamenkovic et al. argue that due to transition metal oxides next to Pt atoms the surface coverage of OH_{ad} compared to pure Pt is significantly reduced [23]. Due to this reduction in surface coverage more active surface is available. They hypothesize that there may be a repulsive interaction between Pt-OH and the metal oxide. Cobalt (or nickel) seems to act as sacrifice element.

On the other hand they observed similar activity enhancement on core-shell-nanoparticles (PtM in the core, Pt at the surface). Because the explanation above is obsolete in this case they further argue that the increased electrocatalytic activity can only be explained by changes in the electronic structure of the surface atoms (see section 1.6.2.4).

1.6.2.3 Roughening of the surface structure

Gasteiger et al. and *Paffett* explain the increased activity of alloy catalysts by a roughening effect when the less noble metal is dissolved in acidic conditions. Due to this dissolution the ECSA increases [14,24].

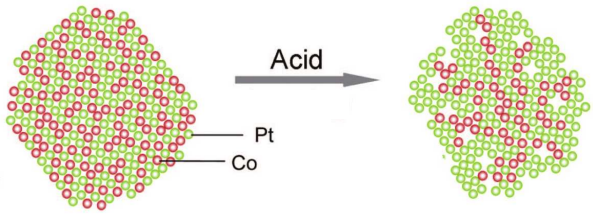

Figure 9: Proposed scheme of the surface roughening effect in acidic conditions [25]

Paffett defends this explanation by the finding that $PtCr_4$ has a significantly higher ORR current (per area of RDE) while the Tafel slopes for Pt-Cr-alloys and pure Pt catalysts do not differ significantly [24].

1.6.2.4 D-band vacancies

Experiments as well as calculations show a volcano like relationship between the ORR activity on Pt skin surfaces and the adsorption energy of oxygen on platinum or the energy of the d-band center [26].

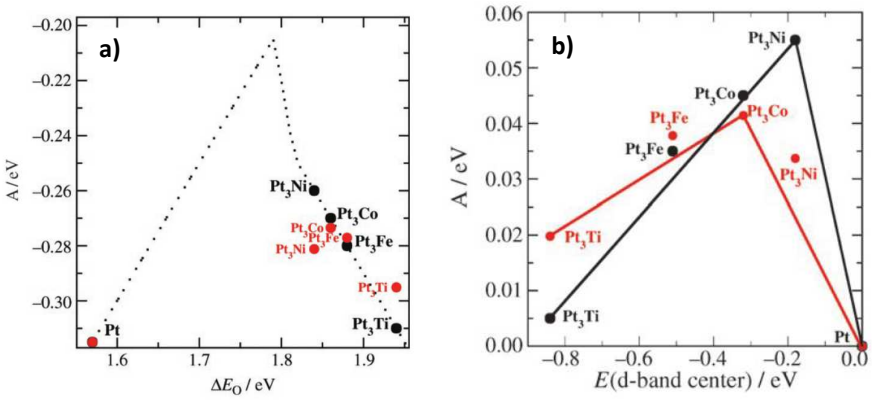

Figure 10: a) ORR activity vs. adsorption energy of oxygen species, b) ORR activity vs. d-band center (results of DFT calculations are shown in black, experimental results in red) [26]

In Figure 10 a) *Stamenkovic et al.* report calculated (black) and measured (red) activities depending on adsorption of oxygen species. On the left side of the diagram oxygen species adsorb too strongly on the surface while on the right side they adsorb too weakly. Calculations (doted line) show that the optimal adsorption energy would be about 0.2 eV weaker than that of pure Pt. Figure 10 b) shows the relationship between the ORR activity and the d-band center relative to platinum. The peak at around -0.2 eV is explained by too strong binding to oxygen on the right side and too weak binding on the left side respectively. If the binding to oxygen is a little too strong (like platinum) the rate limiting step is the removal of reduced oxygen species. In the other case the oxygen adsorption is the rate limiting step [26].

A higher degree of alloying of Pt and Co increases the extent of hybridization of Pt (5d) and Co (3d) and induces an electron transfer from Co to Pt. This electron transfer generates less unfilled d-states and a greater d-band vacancy compared to unalloyed platinum [27]. This effect decreases the bond strength between Pt and O and increases the turnover frequency [28].

2 Experimental

The aim of our investigations is a big scale production process of cathode electrodes for HT-PEMFCs. Our partner, elcomax GmbH Munich, already developed a roll-to-roll process for carbon support materials with a state-of-the-art platinum catalyst (described in Section 1.6.1).

An increase in catalytic activity and stability and a decrease in platinum loading are tried to be achieved by implementing platinum cobalt (alloy) catalysts.

2.1 Sample preparation

Because Co^{2+} salts cannot be reduced by hydrogen (E_0 = -0.28 V) other reducing agents have been investigated [19]: sodium borohydride, formic acid, formaldehyde and ethylene glycol (EG). Atomic ratios Pt:Co of 1:1, 1:3, 1:5 and 1:7 have been tested during the investigations. As Pt precursor hexachloroplatinic acid (H_2PtCl_6) and as Co precursor cobalt nitrate hexahydrate ($Co(NO_3)_2$ $6H_2O$) have been used. A good compromise between solubility of the precursor salts and good moisturing of the hydrophobic GDE was achieved by the solvent mixture water and IPA in a volumetric ratio of 1:1. Temperature and time span of the reduction step have also been optimized.

The manufacturing process was simulated by GDE layer sheets of 2.2x2.2 cm². An appropriate amount of impregnation solution (containing Pt and Co precursors, reducing agent and solvent) was displaced on a GDE sheet resulting in a Pt loading of 1.00 mg Pt/cm² or 1.20 mg Pt/cm². The sheet was dried at 100°C and reduced at various elevated temperatures. The parameters that were optimized are:

- Reducing agent
- Pt:Co ratios
- Temperature of reducing step
- Atmosphere during reduction (air vs. nitrogen)

2.1.1 Stabilization procedures

After identifying optimal combinations of the parameters mentioned above various stabilization strategies were investigated:

- Acid leaching
- Deposition of additional platinum layers
- Temperature treatment
- Temperature treatment with surfactant

The stabilization strategies listed here were carried out standing alone and in combination with each other. The results of these procedures are presented in section 3.

2.1.1.1 Acid leaching

Acid leaching steps were performed in sulfuric acid, nitric acid, hydrochloric acid, acetic acid and phosphoric acid in a mixture of water and IPA (1:1). The GDE sheets were put in a glass beaker and the corresponding diluted acid was added. After 30 minutes of leaching at room temperature the sheets were washed in water and IPA (1:1).

With this step a surface roughening effect that is mentioned in section 1.6.2.3 was achieved. This effect is explained by the dissolution of cobalt in the surface region (a proposed scheme is shown in Figure 9).

2.1.1.2 Deposition of additional platinum layers

After the reduction of various Pt:Co ratios on the GDEs a second Pt or Pt:Co deposition was performed yielding in an overall Pt loading of 1.20 mg/cm^2. With this two-step procedure sort of Pt:Co-core Pt-shell nanoparticles are formed that are more active and more stable. A protecting layer of platinum over the non-noble cobalt could explain an increased stability.

2.1.1.3 Temperature Treatment

An additional annealing step has been reported to have an influence on the surface structure and therefore a positive influence on electrocatalytic activity [22]. The temperature treatment was carried out between 200°C and 300°C for one hour in nitrogen atmosphere.

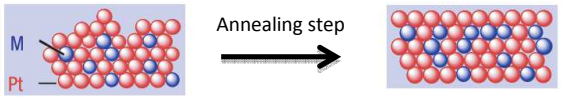

Figure 11: Proposed scheme of surface arrangement during annealing step [22]

2.1.1.4 Temperature Treatment with surfactant

Additionally to the temperature treatment surfactants were added to prevent the nanoparticles from agglomeration. In the manufacturing process it would be practical, if the surfactant can be removed at the end of this step thermally. To determine the decomposition temperature and/or the boiling point of the surfactants *Brij30, Brij56* and *Triton X-100* we performed thermo gravimetric analysis (TGA) of our samples.

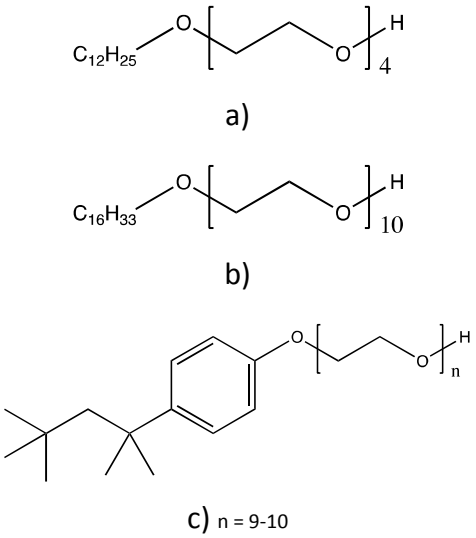

Figure 12: Structure of a) Brij30; b) Brij56; c) Triton X-100

2.1.2 Preparation for characterization

For the electrochemical characterization (details see section 2.2) a dispersion of the catalyst on carbon support material was prepared in an appropriate amount of IPA. A disk with a diameter of 16 mm was punched out of the 2.2x2.2 cm^2 GDE sheet and dispersed in an ultrasonic bath.

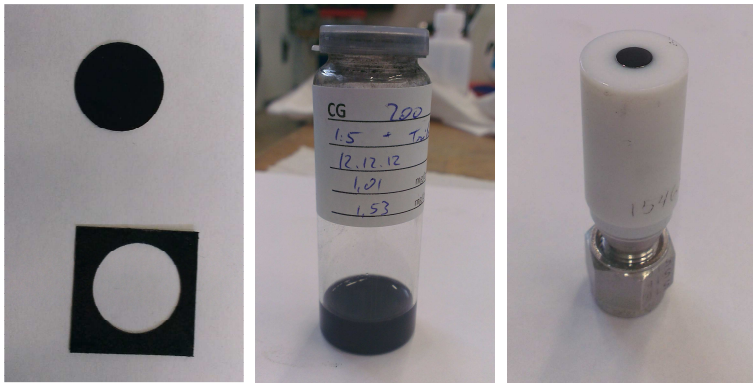

Figure 13: a) a disk of GDE (diameter 16 mm); b) a suspension of a catalyst on high surface carbon in IPA; c) rotating disk electrode (Pine Industries)

For the electrochemical measurements an appropriate amount of the dispersion was transferred on a glassy carbon disk resulting in a platinum loading of 28 µg/cm^2.

2.2 Characterization

Electrochemical characterizations were performed on an Autolab PGSTAT302N potentiostat and a rotator from Pine Industries. These results are divided in staircase (SC)

and linear sweap (LS) measurements because we were not able to perform linear sweap electrochemical measurements during the first months of the project.
As electrolyte a 0.1 molar perchloric acid solution in ultrapure water was used. As reference electrode a hydrogen electrode from gaskatel (HydroFlex) was utilized and a platinated titan rod acted as counter electrode. Our working electrode is a glassy carbon disc from Pine Industries.

2.2.1 Cyclic voltammetry (CV)

A linear potential ramp is applied on the working electrode and the resulting current between working and counter electrode is measured. In general the test setup consists of a three-electrode configuration of working electrode, counter electrode and reference electrode. In most cases aqueous electrolytes are used and the reverse potential is set between oxygen and hydrogen evolution.

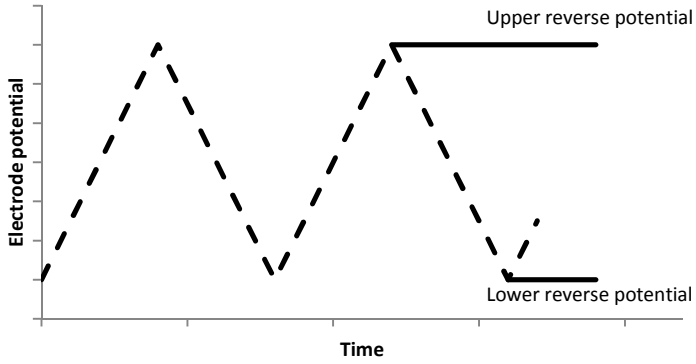

Figure 14: Potential ramp: electrode potential vs. time in a cyclovoltammetric measurement

The most important parameters are the upper and the lower reverse potential and the scan rate. If there is no electrochemical reactive species in the electrolyte, the current from adsorbing and desorbing hydrogen and oxygen on the surface is measured [29]. A typical cyclic voltammogram of a platinum surface in perchloric acid is shown in Figure 15.

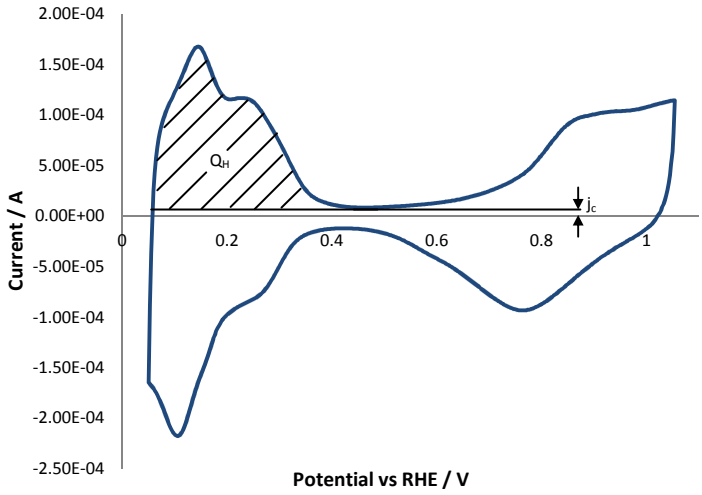

Figure 15: Typical cyclic voltammogram of platinum in perchloric acid

In the region of 0.5 V the current j_c depends on the formation of the electrical double layer. At higher potentials the current represents the formation of a chemisorption layer of oxygen, which results in the evolution of oxygen above 1.6 V. When the potential is reversed, the cathodic peak is formed by the reduction of the oxide layer with a quite high overpotential. Below 0.5 V the formation of a hydrogen chemisorption layer is observed. At around 0 V hydrogen evolution occurs. The most interesting section for our investigation is the region between 0 and 0.5 V with positive scanning direction. Here the oxidation of the hydrogen layer on the platinum surface is observed. From this peak area the ECSA can be calculated [29].

The first peak below 0.2 V is the current from hydrogen chemisorption on Pt(110) surfaces while the second peak between 0.2 and 0.3 V stands for the Pt(100) site [30].

The electrochemical active surface area (ECSA) of the platinum catalyst can be calculated from the area of the peak Q_H [31].

$$Q_H = \int_{\varphi 1}^{\varphi 2} i(\varphi)dt = \frac{1}{\nu}\int_{\varphi 1}^{\varphi 2} i(\varphi)d\varphi \tag{9}$$

$$A_{active} = \frac{Q_H}{210*10^{-6}} \tag{10}$$

$$a_{active} = \frac{A_{active}}{A_{RDE}*l_{Pt}} \tag{11}$$

Q_H	electric charge / C
i	capacitive current / A
dt	time / s
dϕ	voltage / V
v	scan rate / $V \cdot s^{-1}$
A_{active}	aktive surface area / cm^2
a_{active}	specific active surface area / $cm^2 \cdot mg^{-1}$
A_{RDE}	area of electrode / cm^2
l_{Pt}	platinum loading on electrode / $mg \cdot cm^{-2}$

2.2.1.1 Oxygen reduction reaction (ORR)

To measure the activity of the catalyst towards the ORR a CV was recorded in an oxygen saturated electrolyte (example see doted line in Figure 16). Saturation was achieved by bubbling pure oxygen through the electrolyte for about 15 minutes. Comparable ORR activity results are given in terms of specific activity j_k in mA/cm² and mass activity j_{mass} in A/mg Pt (equations 13 and 15). The ORR curve is corrected by subtracting the CV curve with inert electrolyte (see solid line in Figure 16). Equation 12 shows the expression of the kinetic limited current that is valid in the region where $0.1 \cdot i_d < i < 0.8 \cdot i_d$ [17].

$$\frac{1}{i} = \frac{1}{i_k} + \frac{1}{i_d} \tag{12}$$

i	measured current at 0.9 V
i_k	kinetic limited current
i_d	diffusion limited current

The specific activity j_k can be easily calculated (see equation 13). Since the surface area of platinum and the geometrical area of the RDE differ especially in the case of nanocrystalline catalysts j_k has to be corrected by the so-called roughness factor RF [17].

$$j_k = \frac{i_k}{A_{active}} = \frac{i_d * i}{i_d - i} * \frac{1}{RF * A_{RDE}} \tag{13}$$

j_k	specific current density
RF	roughness factor (see below)
A_{RDE}	area of the rotating disk electrode

The roughness factor gives the ratio between the surface area of platinum and the area of the RDE [17].

$$RF = \frac{A_{active}}{A_{RDE}} \tag{14}$$

The mass activity j_{mass} can be calculated according to equation 15 [17].

$$j_{mass} = j_k * \frac{RF}{l_{Pt}} \tag{15}$$

A typical cyclic voltammogram in an oxygen saturated electrolyte is shown in Figure 16. The curve is divided in two regions: the kinetic controlled region above 0.9 V and the diffusion controlled region at lower potentials.

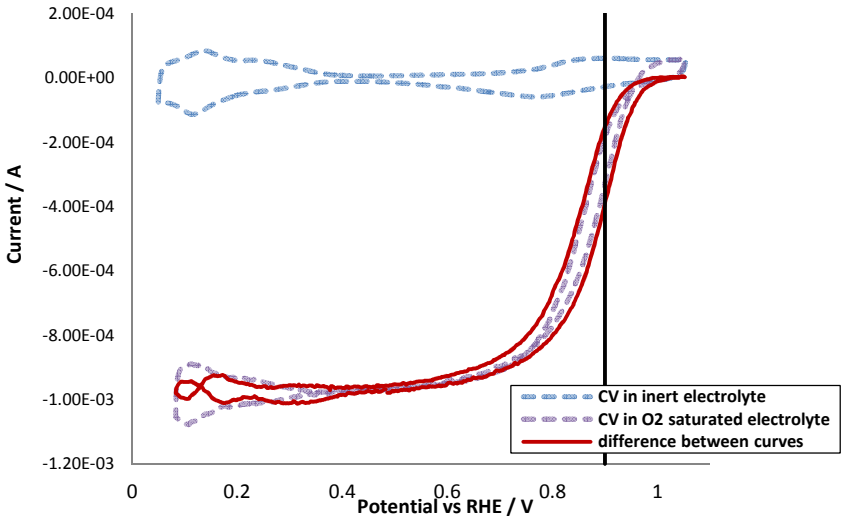

Figure 16: Cyclic voltammogram of platinum in oxygen saturated perchloric acid

2.2.1.2 Accelerated stress test (AST)

Unfortunately a convention for ASTs does not exist. Together with our partner in Munich we designed an AST protocol in form of CV cycles in inert electrolyte to test the stability of the catalyst:

Cycles	555
Upper reverse potential	1.40 V
Lower reverse potential	0.05 V
Scan rate	500 mV * s^{-1}

After 555 cycles a cyclic voltammogram was measured and it was calculated by how much the ECSA decreases.

2.2.2 Thermo gravimetric analysis (TGA)

TGA is characterized by measuring the change of the mass of a sample in dependence of temperature and time. For this purpose an appropriate temperature program is applied while a microbalance is recording the mass change. Typical applications of this method are the determination of boiling points, decomposition temperatures or the mass changes due to oxidation or reduction of the sample. The result of a TGA is usually shown in a diagram with temperature on the horizontal axis and relative mass on the vertical axis (see Figure 17). Our analyses were performed on a NETZSCH STA 449 C (with special thanks to Josefine Hobisch).

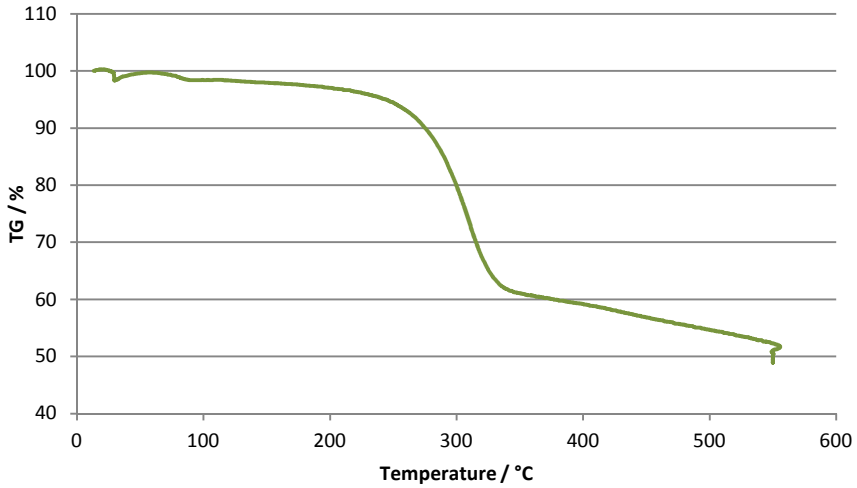

Figure 17: Thermo gravimetric analysis of a catalyst layer with a surfactant

3 Results and Discussion

As mentioned in the previous section the CV results are divided in staircase scan and linear scan measurements. The detailed sample preparation parameters of all results that are presented here are given in the supplementary information (section 6.2).

3.1 Sample preparation

3.1.1 Reducing agents

The use of sodium borohydride, formic acid, formaldehyde and ethylene glycol as reducing agents was investigated (these samples were characterized by CV staircase measurements, see Figure 19).

There are two problems with sodium borohydride: (i) it cannot be combined with the precursors prior to the impregnation because it has too strong reducing properties (this would be quite unpractical for the manufacturing process); (ii) if it is added in an additional step the fast reaction destroys the active layer of our GDE sheets (see Figure 18).

Figure 18: GDE sheet that was treated with sodium borohydride

Using an aldehyde as reducing agent the pH-conditions require being basic. In the case of formic acid a quite big amount of potassium hydroxide has to be added to get a reasonable reactivity. However, since Co^{2+} is not soluble in basic solutions aldehydes are also quite unpractical (instantly a blue precipitation occurs). Results of catalysts that were synthesized with a two-step impregnation are presented in Figure 19.

Ethylene glycol on the other hand can be mixed with the precursors, which allows a one-step impregnation (the reduction occurs at temperatures above 200°C).

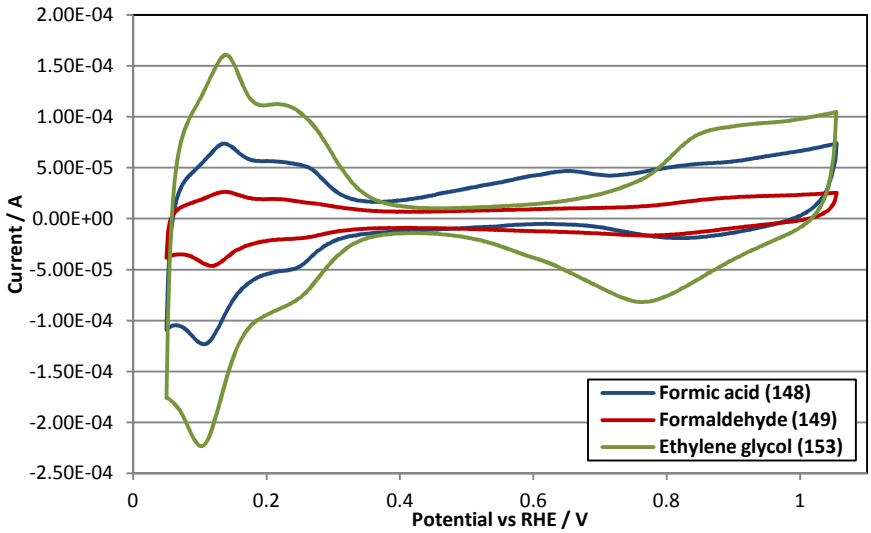

Figure 19: CV of catalysts synthesized with various reducing agents

Table 2: ECSA results of various reducing agents

	ECSA
	cm²/mg Pt
Formic acid **(148)**	**198**
Formaldehyde **(149)**	**67**
Ethylene glycol **(153)**	**534**

All further experiments described in this thesis were carried out using ethylene glycol. The main reason for this decision is that EG is most suitable for the big scale process.

3.1.2 Pt:Co ratios

3.1.2.1 CV staircase measurements

To determine the optimal stoichiometry of platinum and cobalt, catalysts with Pt:Co ratios of 1:1, 1:3, 1:5, 1:7 and 1:10 were synthesized with ethylene glycol at 240°C.

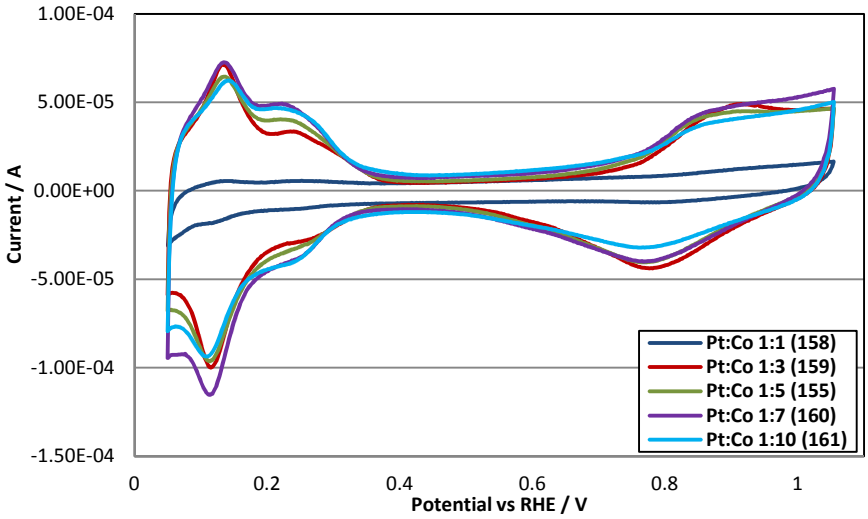

Figure 20: CV of various platinum cobalt ratios

Table 3: ECSA results of various Pt:Co ratios (measured with linear scan CV)

	ECSA
	cm²/mg Pt
Pt:Co 1:1 **(158)**	**15**
Pt:Co 1:3 **(159)**	**172**
Pt:Co 1:5 **(155)**	**191**
Pt:Co 1:7 **(160)**	**225**
Pt:Co 1:10 **(161)**	**193**

Many experiments were conducted to determine the optimal stoichiometry of Pt and Co. Figure 20 shows a representative series of samples with all ratios that were investigated. Because all samples except of the ratio 1:1 seem to have very similar ECSAs the decision was made based on the ORR results. After optimizing the synthesizing procedure the catalysts, especially the Pt:Co ratios of 1:5 and 1:7, showed quite good activities. A maximum of activity could be obtained with the ratio 1:5.

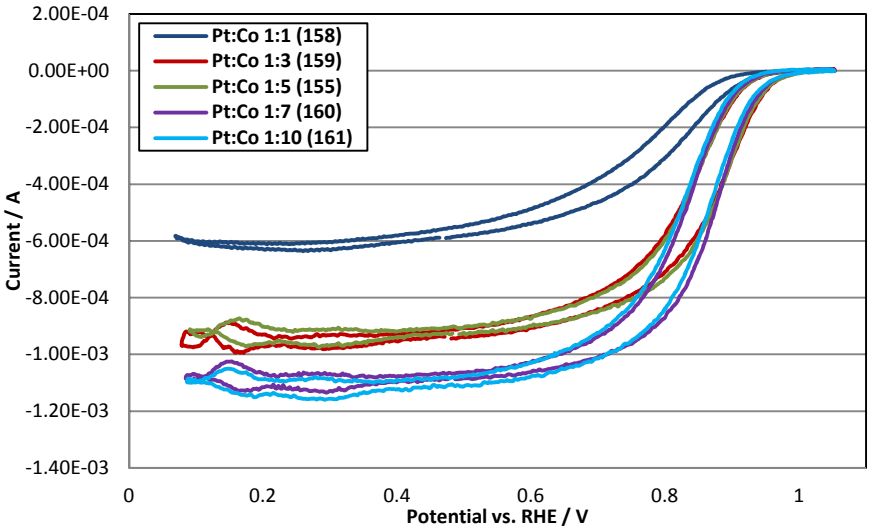

Figure 21: ORR of various platinum cobalt ratios (samples 155, 158-161)

Table 4: ORR activity results of various platinum cobalt ratios (samples 155, 158-161)

	Specific activity	Mass activity
	mA/cm²	**A/mg Pt**
Pt:Co 1:1 **(158)**	**0.859**	**0.013**
Pt:Co 1:3 **(159)**	**0.460**	**0.079**
Pt:Co 1:5 **(155)**	**0.431**	**0.082**
Pt:Co 1:7 **(160)**	**0.307**	**0.069**
Pt:Co 1:10 **(161)**	**0.294**	**0.057**

The ORR results of the ratios 1:3, 1:5 and 1:7 are quite similar (see Figure 21). Because the ECSA results as well as the ORR results do not allow a definite decision, more experiments were done by CV linear scan measurements.

3.1.2.2 CV linear scan measurements

Catalysts with platinum cobalt ratios of 1:1, 1:3, 1:5 and 1:7 were synthesized with ethylene glycol at 230°C.

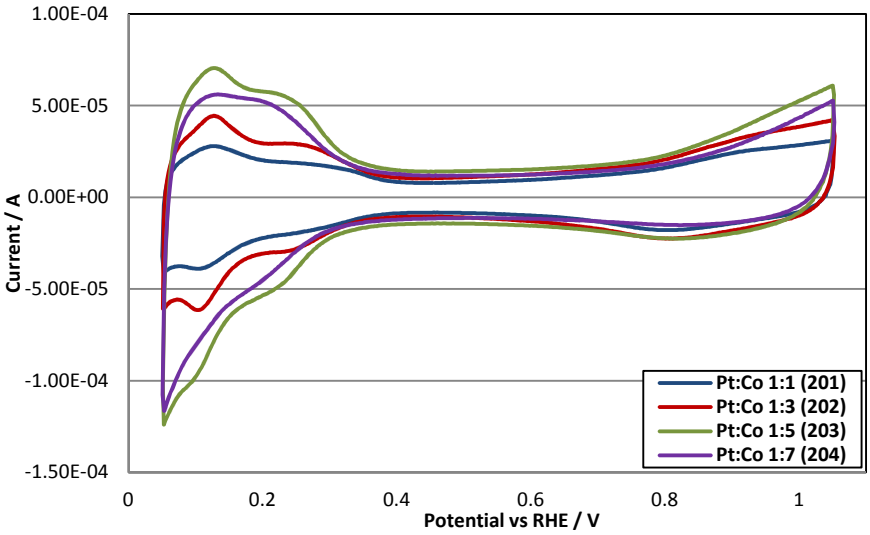

Figure 22: CV (linear scan) of various platinum cobalt ratios (201-204)

Table 5: ECSA results of various Pt:Co ratios (measured with linear scan CV)

	ECSA
	cm²/mg Pt
Pt:Co 1:1 **(201)**	**79**
Pt:Co 1:3 **(202)**	**127**
Pt:Co 1:5 **(203)**	**243**
Pt:Co 1:7 **(204)**	**183**

As can be seen in Figure 22 at about 0.8 V there is no platinum oxide peak. This peak and the activity concerning the ORR only evolve if the samples are cleaned by at least 200 CV staircase cycles with a scan rate of 0.5 V/s. If these cycles are performed by linear scan methods the ORR activity does not evolve, so obviously the linear scan cycles do not exhibit the same cleaning properties than the staircase methods, hence the catalyst surface remains unavailable for oxygen molecules. Because of this observation all cleaning cycles are executed with staircase methods (see section 6.2).

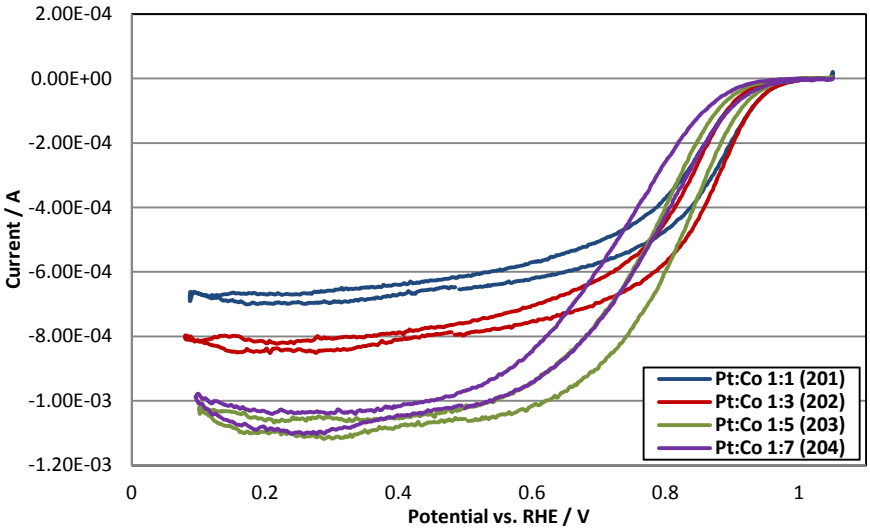

Figure 23: ORR of various platinum cobalt ratios (samples 201-204)

Table 6: ORR activity results of various platinum cobalt ratios (samples 201-204)

	Specific activity	Mass activity
	mA/cm²	**A/mg Pt**
Pt:Co 1:1 **(201)**	**0.602**	**0.048**
Pt:Co 1:3 **(202)**	**0.393**	**0.050**
Pt:Co 1:5 **(203)**	**0.115**	**0.028**
Pt:Co 1:7 **(204)**	**0.093**	**0.017**

The activity concerning the ORR of these samples is significantly lower compared to the samples presented in section 3.1.2.1 (see Figure 23 and Table 6). The reason is explained above and can also be seen by the missing Pt-O peak in Figure 22 at about

0.8 V. Because of this observation the activity values of the staircase measurements that are given in Table 4 are more reliable.
The results of the ECSAs confirm our findings of the staircase measurements that the ratios 1:5 and 1:7 are most promising.

3.1.3 Reducing Atmosphere

Oxygen in the atmosphere during the reduction at elevated temperatures forms metal oxides that might have an influence on the catalytic activity and the nanoparticle formation. To investigate this influence several experiments with air or nitrogen atmosphere were conducted.

3.1.3.1 CV staircase measurements

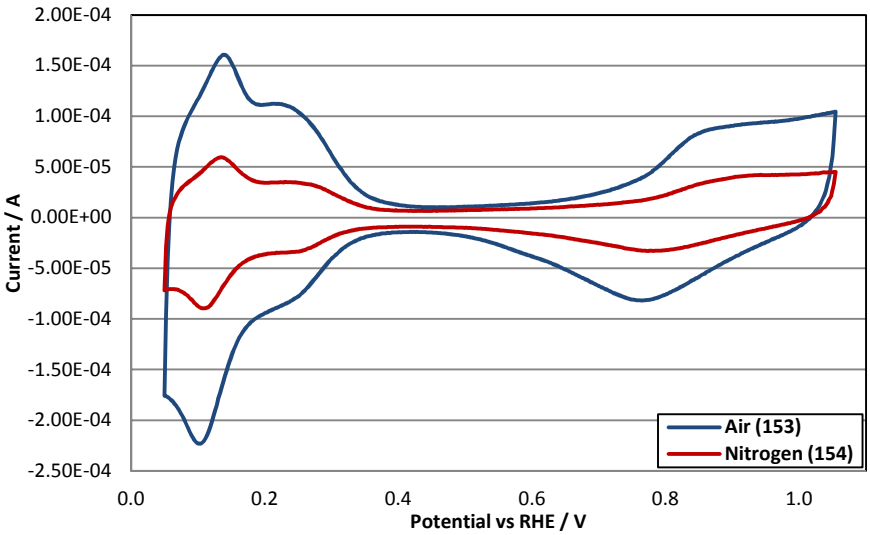

Figure 24: CV of Pt:Co 1:5 catalysts; reduced in air and nitrogen respectively (samples 153-154)

Table 7: ECSA results of Pt:Co 1:5 catalysts; reduced in air and nitrogen respectively (samples 153-154)

	ECSA
	cm²/mg Pt
Air **(153)**	**534**
Nitrogen **(154)**	**177**

As can be seen from these experiments, exemplified in Figure 24, the ECSA is higher if the catalysts are synthesized in air. This observation can be explained by the formation of oxides at the surface in the early stage of the particle formation and that the reduction takes place preferably at sites without oxides. In other words passivation layers inhibit particle growth. Therefore more and smaller particles in catalyst samples are obtained by reduction in air. Surprisingly this effect is not observed any

more if the platinum loading is reduced to 1.00 mg/cm² instead of 1.20 mg/cm² (see samples 209 and 229 in Figure 26).

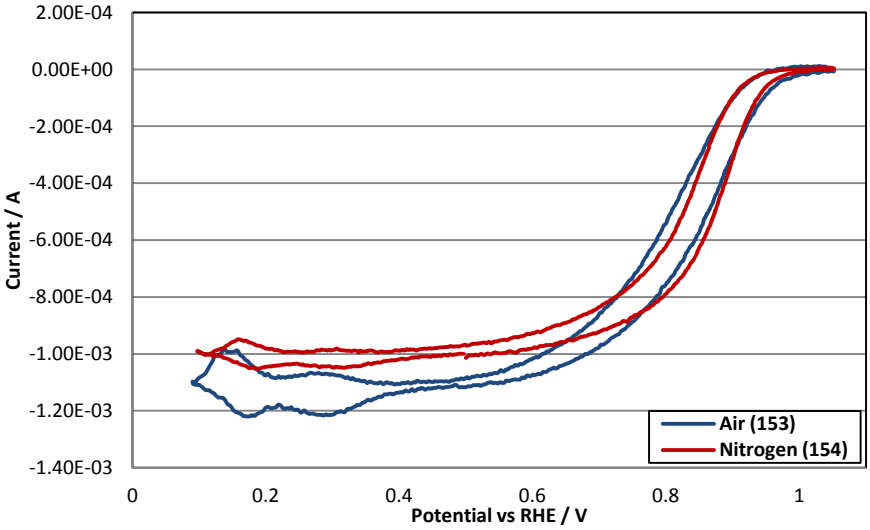

Figure 25: ORR of Pt:Co 1:5 catalysts; reduced in air and nitrogen respectively (samples 153-154)

Table 8: ORR activity results of Pt:Co 1:5 catalysts; reduced in air and nitrogen respectively (153-154)

	Specific activity	Mass activity
	mA/cm²	**A/mg Pt**
Air **(153)**	**0.135**	**0.072**
Nitrogen **(154)**	**0.473**	**0.084**

The ORR of the samples 153 and 154 is a very good example of the particle size effect that is explained in section 1.5.6.1 (see Figure 25). Although the ECSA of sample 153 is three times higher the mass activity of sample 154 is higher. Obviously the particle size effect overcompensates the effect of higher surface areas in this range of particle sizes.

3.1.3.2 CV linear scan measurements

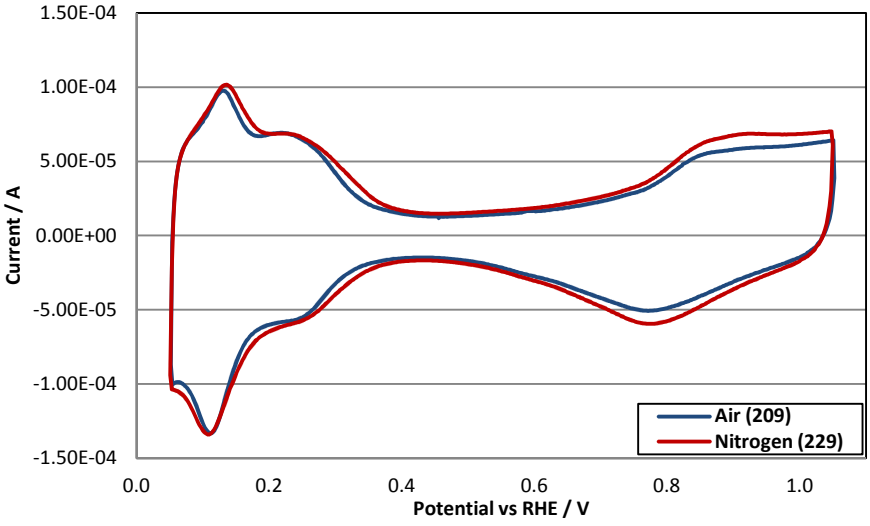

Figure 26: CV of Pt:Co 1:5 catalysts; reduced in air and nitrogen respectively (samples 209 and 229)

Table 9: ECSA results of Pt:Co 1:5 catalysts; reduced in air and nitrogen respectively (samples 209 and 229)

	ECSA
	cm²/mg Pt
Air **(209)**	**304**
Nitrogen **(229)**	**331**

By optimizing the deposition parameters in nitrogen the ECSA can be improved significantly. Samples 209 and 229 are presented here to point out this observation (see Figure 26). In this case the ECSA is even higher in the case of inert atmosphere.

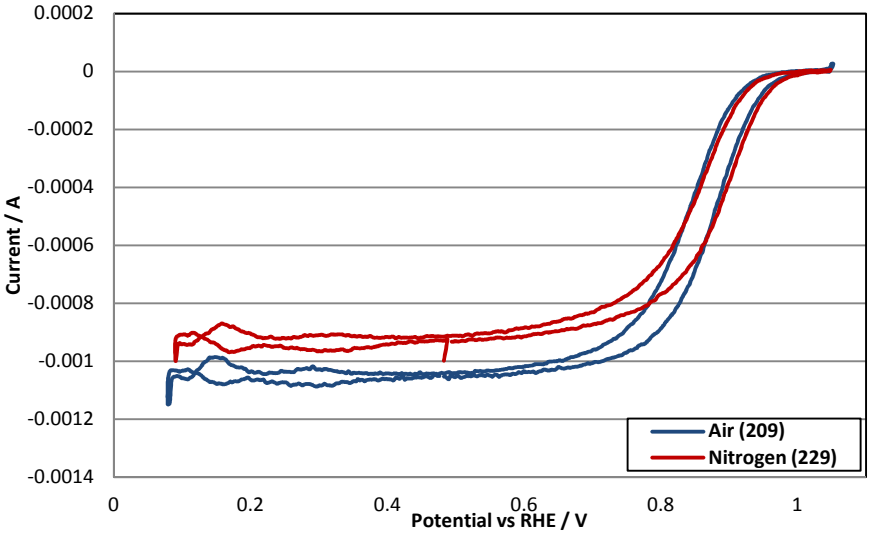

Figure 27: ORR of Pt:Co 1:5 catalysts; reduced in air and nitrogen respectively (samples 209 and 229)

Table 10: ORR activity results of Pt:Co 1:5 catalysts; reduced in air and nitrogen respectively (samples 209 and 229)

	Specific activity	Mass activity
	mA/cm²	**A/mg Pt**
Air **(209)**	**0.276**	**0.084**
Nitrogen **(229)**	**0.331**	**0.109**

A higher activity of catalysts fabricated in inert atmosphere was observed (see Figure 27). Hence the formation of oxides seems to have a negative influence on the catalytic activity.

Another reason for the use of nitrogen for all further investigations is that the synthesis is more reliable. The synthesis in air is very sensible and failed several times (example see Figure 28).

Figure 28: GDE sheet with catalyst that was reduced in air

3.1.4 Reducing Temperature

Experiments showed that the reducing temperature has to be at least 220°C if ethylene glycol is used as reducing agent. To find the optimal temperature the same impregnation solution with the Pt:Co ratio of 1:5 was reduced at the temperatures 220°C, 230°C, 240°C and 250°C.

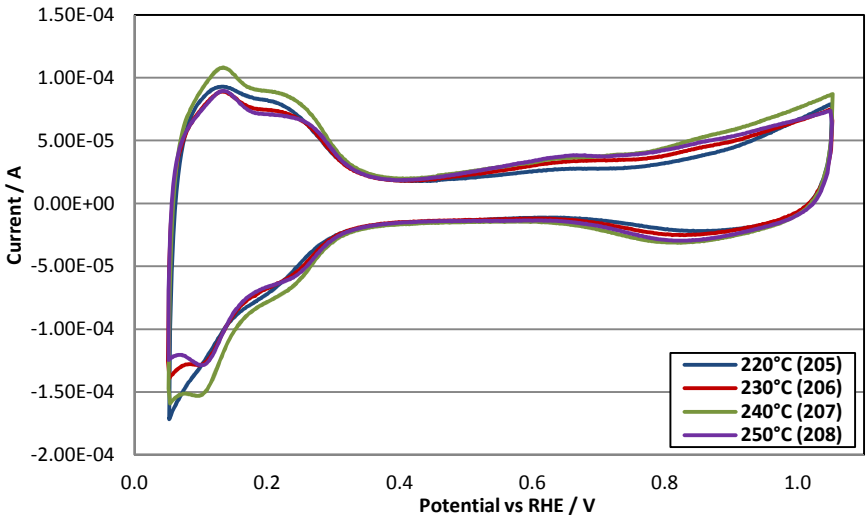

Figure 29: CV of Pt:Co 1:5 catalysts; reduced at various temperatures (samples 205-208)

Table 11: ECSA results of various reducing temperatures (samples 205-208)

	ECSA
	cm²/mg Pt
220°C **(205)**	**304**
230°C **(206)**	**274**
240°C **(207)**	**343**
250°C **(208)**	**273**

Several series of experiments were conducted to determine the reducing temperature that yields to the most active catalyst. The samples 205-208 show that the temperature has only a small influence on the ECSA (see Figure 29 and Table 11). In these series the same effect of no platinum oxide peak than in the samples 201-204 can be observed. These samples were also prepared with linear scan cleaning cycles instead of staircase cleaning cycles.

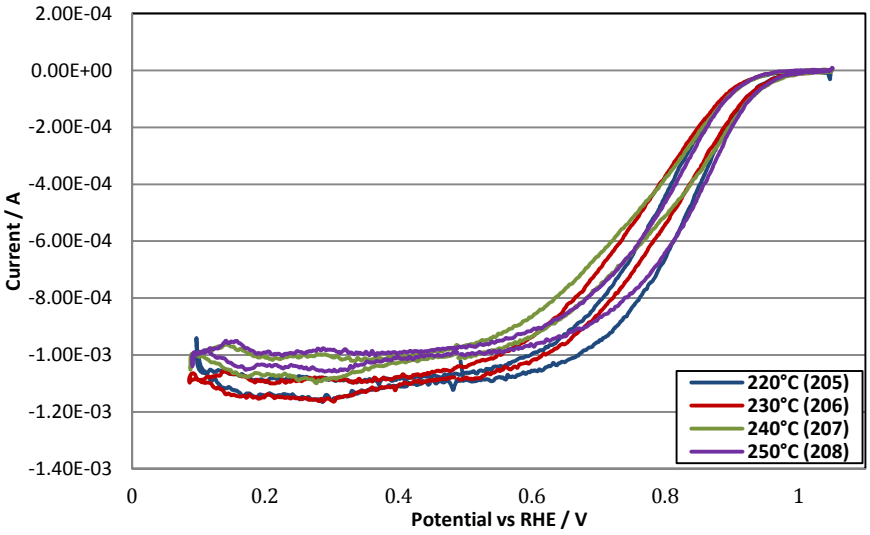

Figure 30: ORR of Pt:Co 1:5 catalysts; reduced at various temperatures (samples 205-208)

Table 12: ORR activity results of various reducing temperatures (samles 205-208)

	Specific activity	Mass activity
	mA/cm²	**A/mg Pt**
220°C **(205)**	**0.120**	**0.037**
230°C **(206)**	**0.123**	**0.034**
240°C **(207)**	**0.117**	**0.040**
250°C **(208)**	**0.164**	**0.045**

The influence on the ORR activity is also negligible in this series (see Figure 30 and Table 12). The results of these samples show a poor activity because of the linear scan CV cleaning cycles.

Considering all results concerning the temperature the reduction at 240°C seems to be optimal for the ECSA and ORR activity. Therefore the catalysts were synthesized at 240°C for all further investigations.

3.2 Sample stabilization

As benchmark for our stabilization procedures we use on the one hand the platinum standard from our partner elcomax GmbH Munich (sample ÜKH41) and on the other hand our platinum cobalt catalysts that were not stabilized (sample 155).

It was started with leaching the samples with various acids. After optimizing this step it was continued with the other strategies in combination with acid leaching. The stabilization is measured and compared by conducting the AST cycles (see section 2.2.1.2) and calculating the ECSA and the relative loss during these cycles. The non-stabilized samples lost 71 % (sample 155) and 61 % (sample ÜKH41) of their ECSA by measuring the cyclic voltammogram with staircase measurements and 49 % (sample ÜKH41) by doing the measurement with linear scan methods.

The ECSA after each cycle and the relative loss in respect to the initial area are given in tables next to the graph. All AST cycles are conducted by using CV staircase methods.

3.2.1 Benchmark for stabilization

Non-stabilized Pt:Co 1:5 and Pt standard catalysts acted as benchmark for our stabilization procedures. Results of the samples 155 and ÜKH41 are presented in Figure 31, Figure 32, Figure 33 and Table 13, Table 14, Table 15.

3.2.1.1 CV staircase measurements

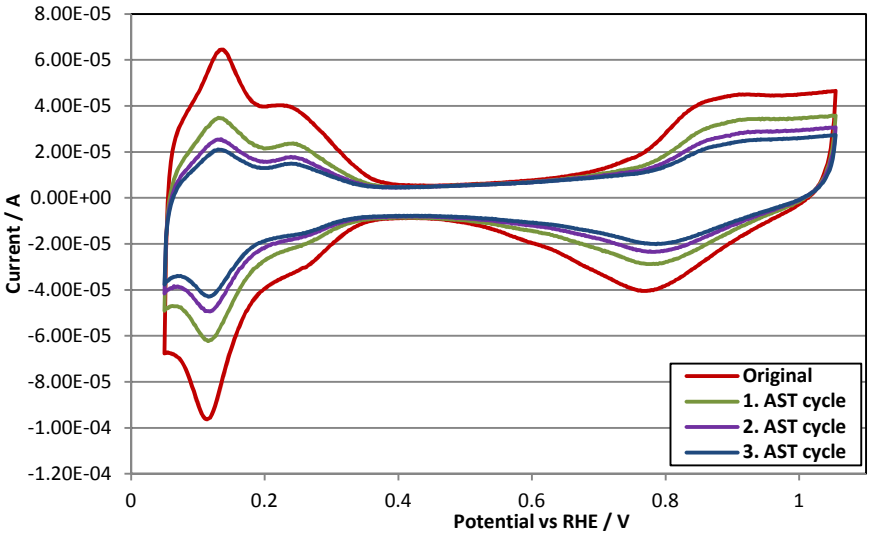

Figure 31: CV of non-stabilzed Pt:Co 1:5 catalyst before and after AST (sample 155)

Table 13: Relative ECSA loss during AST cycles (sample 155).

	ECSA	Relative loss
	cm²/mg Pt	**%**
Original	**191**	**-**
555 AST cycles	**93**	**51 %**
1110 AST cycles	**68**	**65 %**
1665 AST cycles	**55**	**71 %**

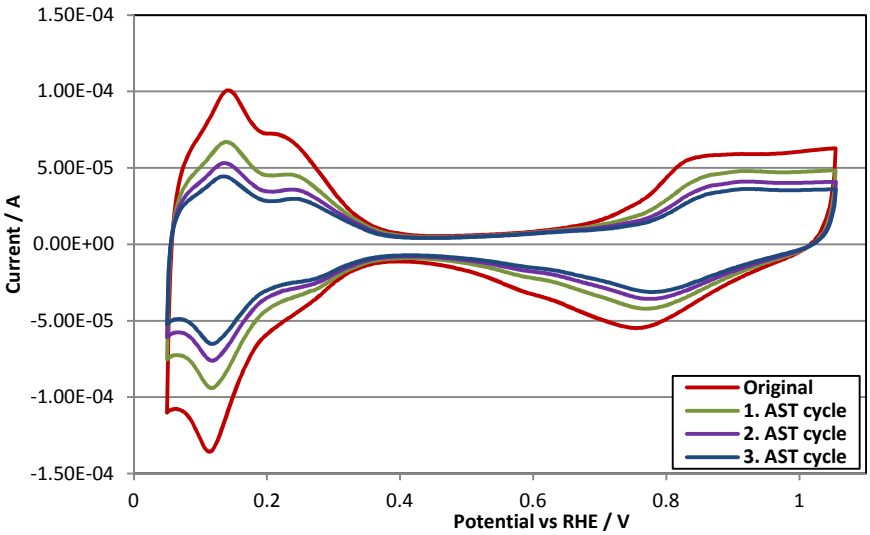

Figure 32: CV of non-stabilzed Pt standard catalyst before and after AST (sample ÜKH41)

Table 14: Relative ECSA loss during AST cycles (sample ÜKH41)

	ECSA	Relative loss
	cm²/mg Pt	**%**
Original	**303**	**-**
555 AST cycles	**193**	**36**
1110 AST cycles	**149**	**51**
1665 AST cycles	**120**	**61**

The benchmarks for the staircase measurements of our stabilization procedures show quite high ECSA losses (71 and 61 %). The biggest loss is observed after the first cycle and is associated with particle agglomeration that occurs preferably with smaller particles. There seem to be kind of a maximum of particle size at which agglomeration stops. Long-time AST cycling is necessary to proof this assumption.

3.2.1.2 CV linear scan measurements

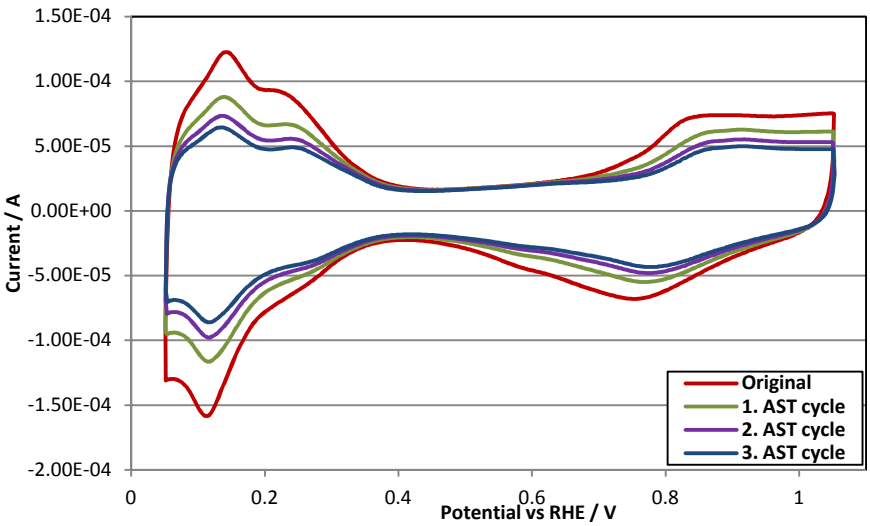

Figure 33: CV of non-stabilzed Pt standard catalyst before and after AST (sample ÜKH41)

Table 15: Relative ECSA loss during AST cycles (sample ÜKH41)

	ECSA	Relative loss
	cm²/mg Pt	**%**
Original	**372**	**-**
555 AST cycles	**275**	**26**
1110 AST cycles	**227**	**39**
1665 AST cycles	**190**	**49**

If the ECSA is measured with linear scan methods the relative loss is a little smaller. In principle the results show the same characteristics than staircase methods.

3.2.2 Acid leaching

3.2.2.1 CV staircase measurements

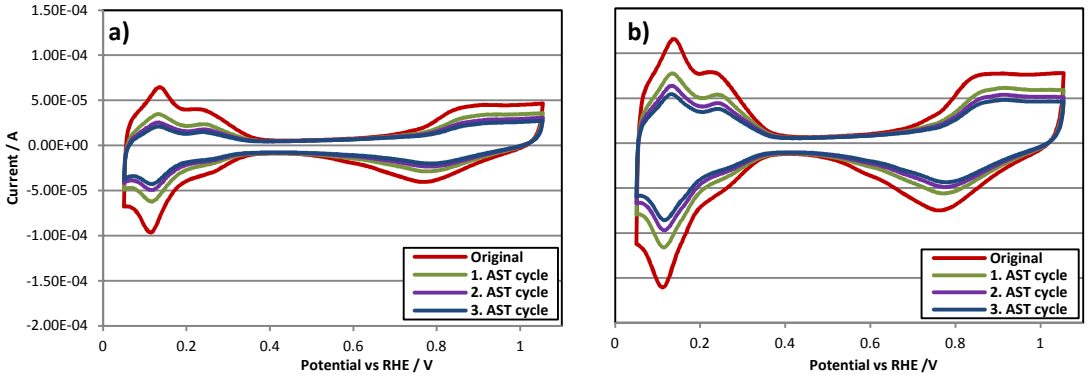

Figure 34: CVs of Pt:Co 1:5 catalysts before and after AST; a) non-stabilized sample (sample 155); b) stabilized by acid leaching with H_2SO_4 (sample 156)

Table 16: ECSA of Pt:Co 1:5 catalysts before and after AST (samples 155 and 156)

	155	155	156	156
	-	-	H_2SO_4	H_2SO_4
	cm²/mg Pt	**rel. loss**	**cm²/mg Pt**	**rel. loss**
Original	**191**	**-**	**380**	**-**
555 AST cycles	**93**	**51 %**	**234**	**38 %**
1110 AST cycles	**68**	**65 %**	**194**	**49 %**
1665 AST cycles	**55**	**71 %**	**174**	**54 %**

The first results of the acid leaching step with 10%vol H_2SO_4 were quite promising. A significant increase of stability and ECSA can be achieved (see Figure 34 and Table 16). This increase can be explained by the surface roughening effect that is explained in section 1.6.2.3.

3.2.2.2 CV linear scan measurements

To compare the effect of different acids on the catalysts during the leaching step of 30 minutes, five identical Pt:Co 1:5 catalysts were prepared and treated with H_2SO_4, HCl, HNO_3, H_3PO_4 and HAc (10 %vol each).

The main influence of different acids is assumed to be the affinity of the anion to the surface of the catalyst. As described in section 1.5.6.1 every anion has a different affinity to the different surface sites. In this respect it is reasonable that the anions of nitric acid and hydrochloric acid should have no or little influence because our precursor salts have the same anions, i.e., chloride and nitrate.

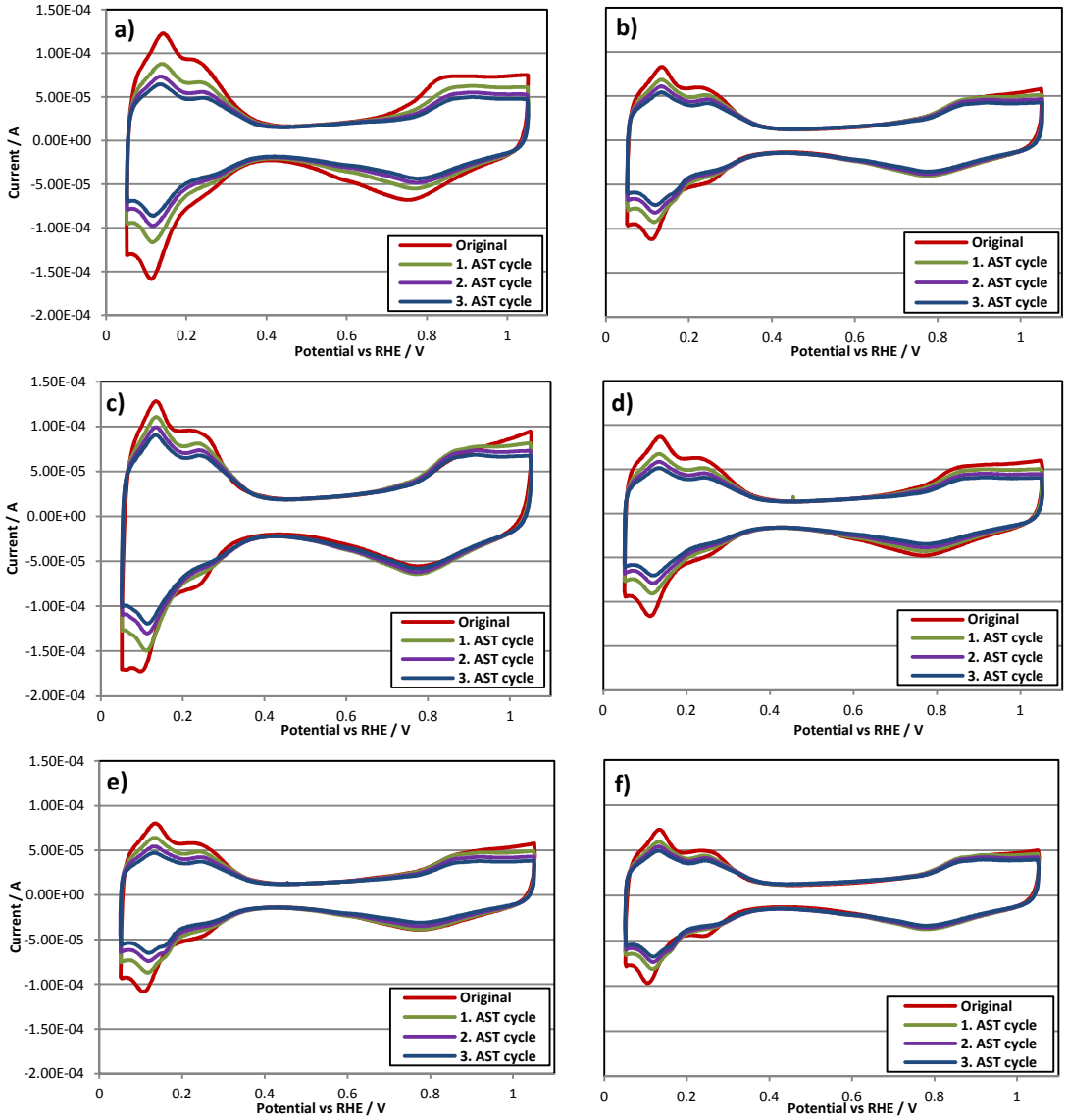

Figure 35: CVs of Pt:Co 1:5 catalysts before and after AST; a) non-stabilized sample (ÜKH41); b) stabilized by acid leaching with H_2SO_4 (211); c) stabilized by acid leaching with HCl (212); d) stabilized by acid leaching with HNO_3 (213); e) stabilized by acid leaching with H_3PO_4 (214); f) stabilized by acid leaching with CH_3COOH (215)

Table 17: ECSAs of acid leached catalysts before and after AST (samples 211-215)

	ÜKH41	211	212	213	214	215
	-	H_2SO_4	HCl	HNO_3	H_3PO_4	CH_3COOH
	cm²/mg Pt					
Original	**372**	**247**	**406**	**288**	**248**	**231**
555 AST cycles	**275**	**221**	**361**	**248**	**217**	**199**
1110 AST cycles	**227**	**195**	**319**	**221**	**199**	**185**
1665 AST cycles	**190**	**182**	**295**	**179**	**158**	**173**

Table 18: Relative ECSA loss during AST (samples 211-215)

	ÜKH41	211	212	213	214	215
	-	H_2SO_4	HCl	HNO_3	H_3PO_4	CH_3COOH
	Relative loss / %					
Original	-	-	-	-	-	-
555 AST cycles	**26**	**10**	**11**	**14**	**12**	**14**
1110 AST cycles	**39**	**21**	**21**	**23**	**20**	**20**
1665 AST cycles	**49**	**27**	**27**	**38**	**36**	**25**

The results confirmed the assumption that HCl and HNO_3 are most promising in terms of ECSA (see Figure 35 and Table 18). Since hydrochloric acid has also quite good results in stability, replacing $Co(NO_3)_2$ with $CoCl_2$ would be the next obvious step.

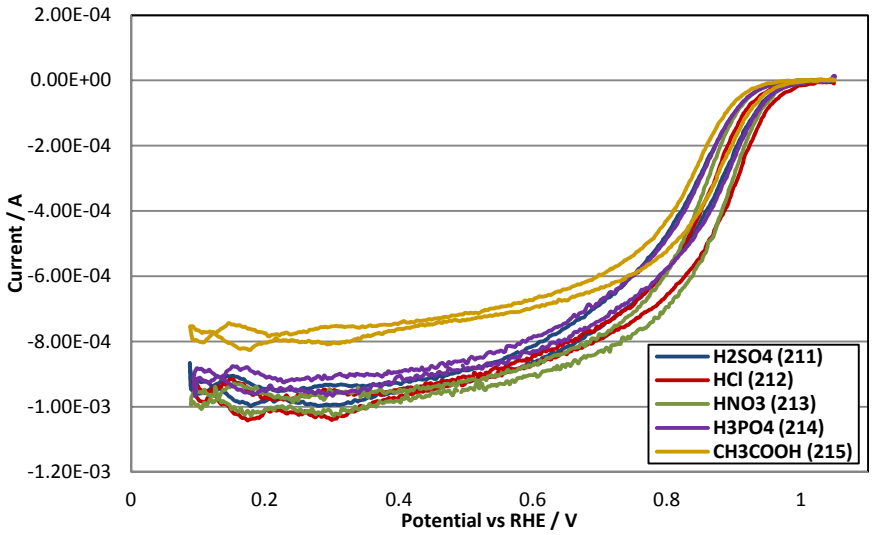

Figure 36: ORR of acid leached Pt:Co 1:5 catalysts (samples 211-215)

Table 19: ORR activity results of acid leached catalysts (samples 211-215)

	Specific activity	Mass activity
	mA/cm²	A/mg Pt
H_2SO_4 (211)	**0.213**	**0.053**
HCl (212)	**0.215**	**0.087**
HNO_3 (213)	**0.256**	**0.074**
H_3PO_4 (214)	**0.229**	**0.057**
CH_3COOH (215)	**0.177**	**0.044**

The ORR results also confirm our hypothesis concerning the anions (see Figure 36 and Table 19). The higher activity can be explained by the higher availability of the active sites for the reaction. By leaching the catalysts with acids other than HCl and HNO_3 additional anions are added to our samples. These anions adsorb to the surface and block the catalytic active area.

3.2.3 Additional platinum layer

The strategies *adding an additional platinum layer* and *annealing* were carried out after an acid leaching step with hydrochloric acid and sulfuric acid respectively. An additional reducing step yields in kind of Pt:Co core Pt shell nanoparticles.

3.2.3.1 CV staircase measurements

The samples 162-165 were leached with 10% H_2SO_4 after the first and/or the second reduction step (details see Table 20). After the first step the platinum loading of samples 162-164 was exactly half of the final loading (0.60 mg Pt/cm² per step). The sample 165 was prepared by reducing 1.01 mg Pt/cm² during the first step and only 0.12 mg Pt/cm² during the second reduction.

Table 20: Sample preparation sequence (samples 162-165)

	1. step	2. step	3. step	4. step
162	**Pt:Co 1:5 reduction**	**Acid leaching**	**Pt:Co 1:3 reduction**	**-**
163	**Pt:Co 1:5 reduction**	**Acid leaching**	**Pt:Co 1:3 reduction**	**Acid leaching**
164	**Pt:Co 1:5 reduction**	**Pt:Co 1:3 reduction**	**Acid leaching**	**-**
165	**Pt:Co 1:5 reduction**	**Acid leaching**	**Pt reduction**	**-**

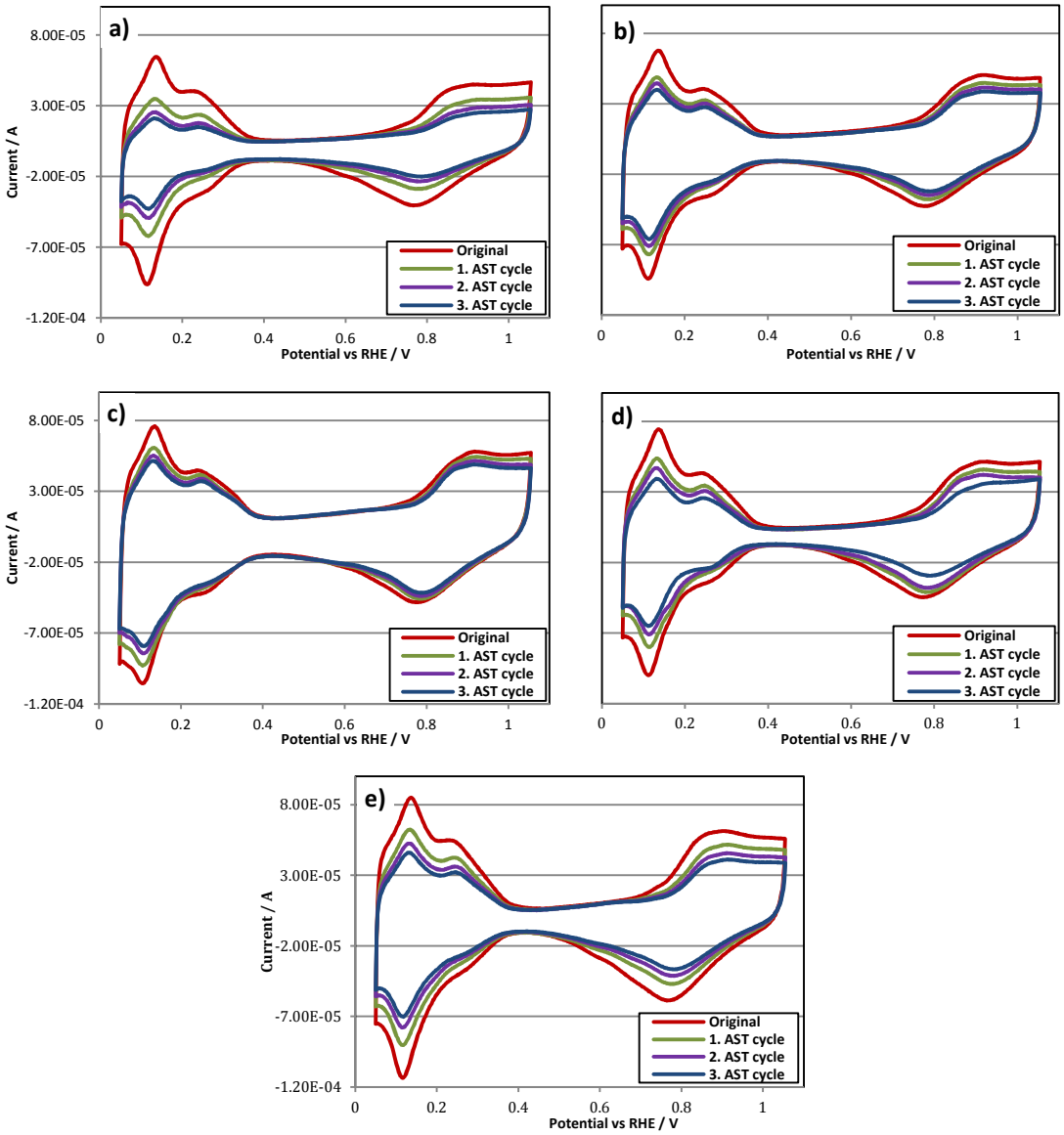

Figure 37: CVs of Pt:Co 1:5 catalysts before and after AST; a) non-stabilized sample (155); b) stabilized by acid leaching with H_2SO_4 and additional Pt-Co layer (162); c) stabilized by acid leaching with H_2SO_4 and additional Pt-Co layer (163); d) stabilized by acid leaching with H_2SO_4 and additional Pt-Co layer (164); e) stabilized by acid leaching with H_2SO_4 and additional Pt layer (165)

Table 21: ECSA of stabilized catalysts before and after AST (samples 155, 162-165)

	155	162	163	164	165
	cm²/mg Pt				
Original	**191**	**199**	**225**	**230**	**279**
555 AST cycles	**93**	**161**	**196**	**161**	**210**
1110 AST cycles	**68**	**135**	**170**	**140**	**180**
1665 AST cycles	**55**	**122**	**160**	**118**	**159**

Table 22: Relative ECSA loss during ASTs (155, 162-165)

	155	162	163	164	165
	Relative loss / %				
Original	-	-	-	-	-
555 AST cycles	**51**	**19**	**13**	**30**	**25**
1110 AST cycles	**65**	**32**	**24**	**39**	**35**
1665 AST cycles	**71**	**39**	**29**	**49**	**43**

These experiments showed that the most promising strategy considering the ECSA is adding a pure platinum layer (see Figure 37 and Table 21). The highest stability could be achieved by leaching the catalysts after both reduction steps (sample 163).

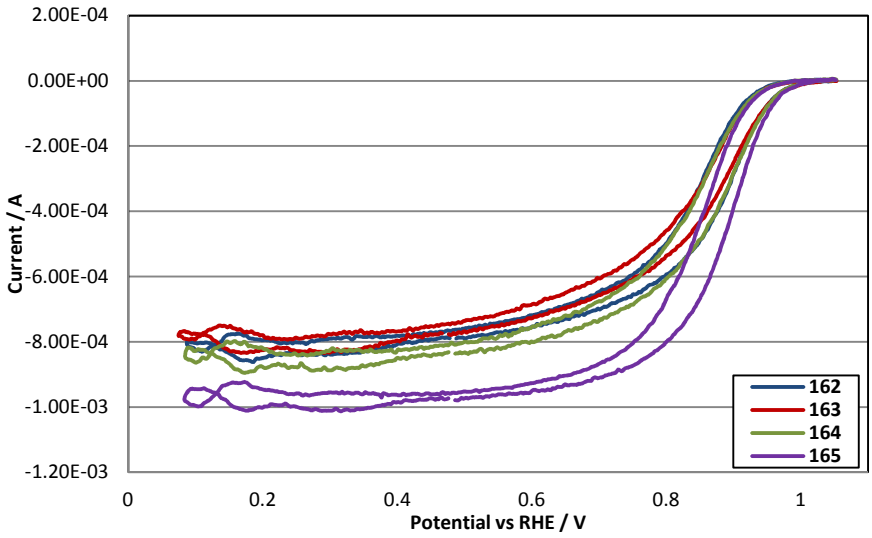

Figure 38: ORR of samples with 2nd reduction step (162-165)

Table 23: ORR activity results of samples with 2nd reduction step (162-165)

	Specific activity	Mass activity
	mA/cm²	A/mg Pt
162	**0.382**	**0.076**
163	**0.281**	**0.063**
164	**0.326**	**0.075**
165	**0.421**	**0.117**

The measurements of the catalyst activity confirm pure platinum deposition to be most promising (see Figure 38). In general we expect increased catalytic activity of nanoparticles with a platinum shell because of changed electronic properties that are explained by cobalt atoms in the core of the particle (see section 1.6.2.4).

Based on these findings it was carried on preparing the samples 216 and 217 with a pure platinum and a Pt:Co 3:1 shell. Here 1.00 mg Pt/cm² was reduced during the first reduction step and only 0.20 mg Pt/cm² was used to form the platinum shell. Acid leaching steps were carried out with hydrochloric acid.

3.2.3.2 CV linear scan measurements

Table 24: Sample preparation sequence (samples 216 and 217)

	1.step	2. step	3. step
Pt-shell **(216)**	**Pt:Co 1:5 reduction**	**Acid leaching**	**Pt reduction**
Pt:Co 3:1-shell **(217)**	**Pt:Co 1:5 reduction**	**Acid leaching**	**Pt:Co 3:1 reduction**

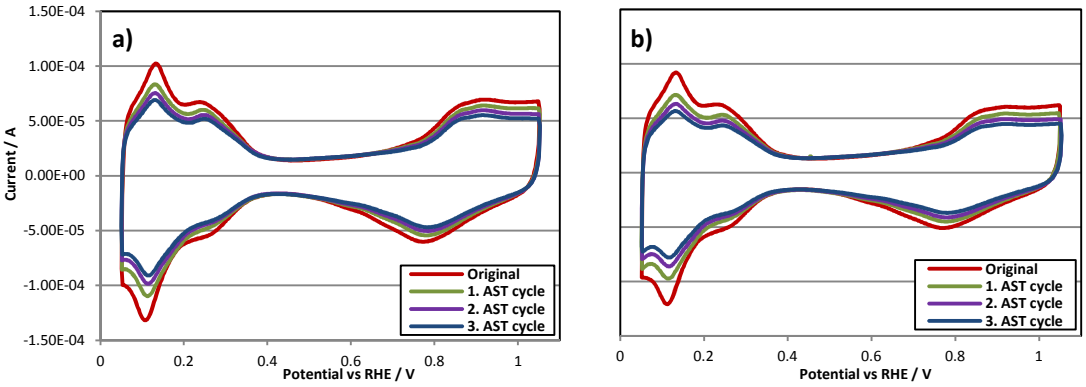

Figure 39: CVs of samples with 2nd reduction step before and after AST; a) sample 216; b) sample 217

Table 25: ECSAs of samples with 2nd reduction step before and after AST (samples 216-217)

	216	216	217	217
	Pt-shell	Pt-shell	Pt:Co 3:1-shell	Pt:Co 3:1-shell
	cm²/mg Pt	**rel. loss / %**	**cm²/mg Pt**	**rel. loss / %**
Original	**256**	**-**	**254**	**-**
555 AST cycles	**233**	**9 %**	**200**	**21 %**
1110 AST cycles	**211**	**18 %**	**186**	**27 %**
1665 AST cycles	**196**	**24 %**	**153**	**40 %**

The ECSA of both samples is quite similar while the sample with the platinum shell is more stable (see Figure 39 and Table 25). Also the platinum amount of both steps seems to be optimal with major quantity within the first reduction. This finding can be explained by the formation of thin platinum shell layers on the nanoparticles.

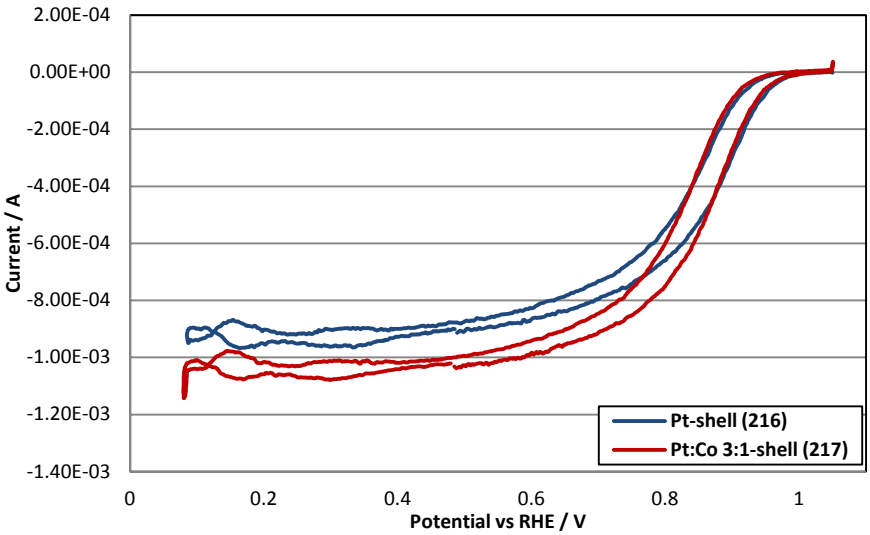

Figure 40: ORR of samples with 2nd reduction step (samples 216-217)

Table 26: ORR activity results of samples with 2nd reduction step (samples 216-217)

	Specific activity	Mass activity
	mA/cm²	**A/mg Pt**
Pt-shell **(216)**	**0.319**	**0.079**
Pt:Co 3:1-shell **(217)**	**0.281**	**0.070**

The ORR results show very little difference. The platinum layer is more active and validates the findings from the previous experiments.

This series of experiments confirmed our previous assumption that an additional platinum layer without cobalt is the most promising strategy. Considering all results it is preferable to reduce bigger amounts within the first step (here about 80%).

3.2.4 Temperature treatment

By an additional annealing step after the acid leaching a further increase of stability and activity can be achieved. 60 minute heat treatments were conducted at 200, 250 and 300°C (samples 173-177). With these annealing steps the activity and stability of the catalyst can be influenced based on a reformation of the surface area (details see section 2.1.1.3).

3.2.4.1 CV staircase measurements

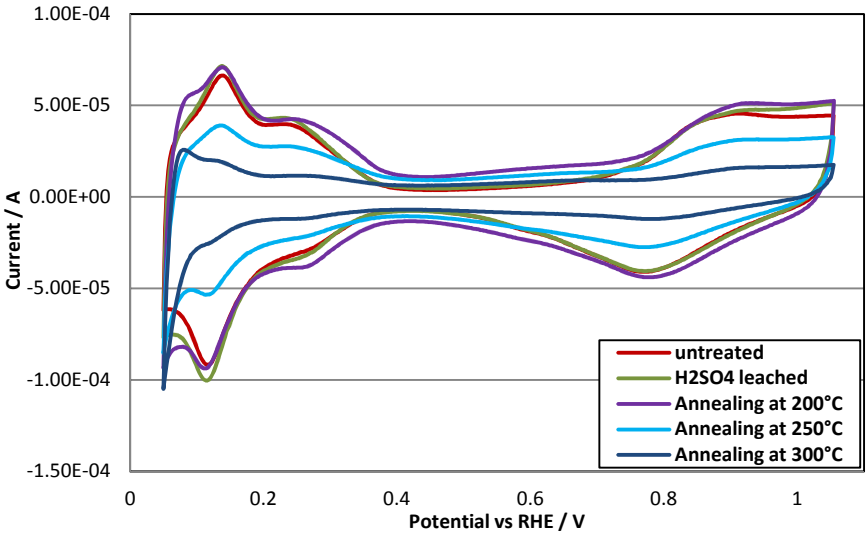

Figure 41: CVs of acid untreated, acid leached and annealed catalysts (samples 173-177)

Table 27: ECSAs of untreated, acid leached and annealed catalysts (samples 173-177)

	ECSA
	cm^2/mg Pt
Untreated **(173)**	**193**
H_2SO_4 **(174)**	**221**
Annealed at 200°C **(175)**	**216**
Annealed at 250°C **(176)**	**126**
Annealed at 300°C **(177)**	**59**

The ECSA results suggest that annealing at 200°C is optimal. At higher temperatures the nanoparticles agglomerate and most of the ECSA gets lost (see Figure 41 and Table 27). To prevent the particles from agglomeration, surfactants were added as stabilizer.

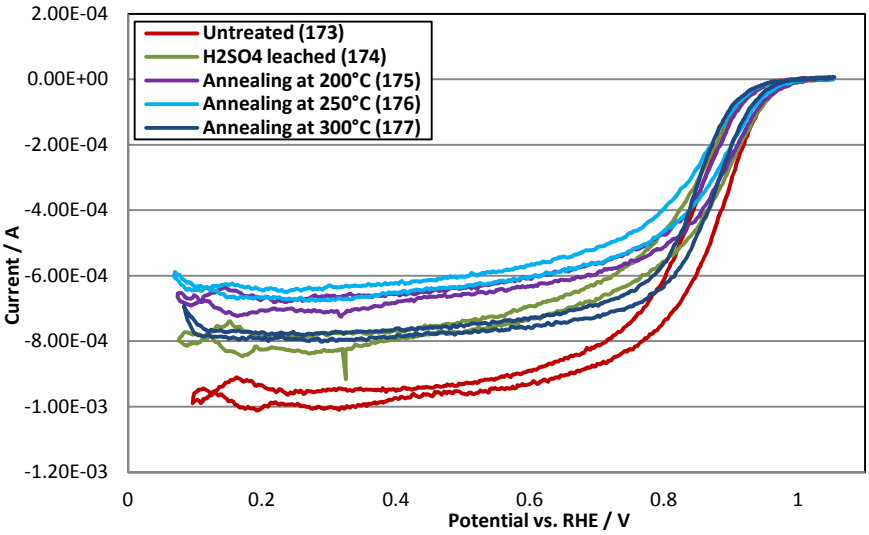

Figure 42: ORR of untreated, H_2SO_4 leached and annealed catalysts (samples 173-177)

Table 28: ORR activity results of untreated, H_2SO_4 leached and annealed catalysts (samples 173-177)

	Specific activity	Mass activity
	mA/cm²	**A/mg Pt**
Untreated **(173)**	**0.423**	**0.082**
H_2SO_4 **(174)**	**0.298**	**0.066**
Annealed at 200°C **(175)**	**0.298**	**0.065**
Annealed at 250°C **(176)**	**0.442**	**0.056**
Annealed at 300°C **(177)**	**0.871**	**0.052**

These annealing steps result in a lowering of the ORR activity as well as a very big loss of ECSA with increasing temperature (see Figure 41 and Figure 42 as well as Table 27 and Table 28). More results from samples with surfactants as stabilizers are presented below (see section 3.2.5).

3.2.5 Temperature treatment with surfactant

The surfactants *Brij30, Brij56* and *Triton X-100* were used.

3.2.5.1 CV staircase measurements

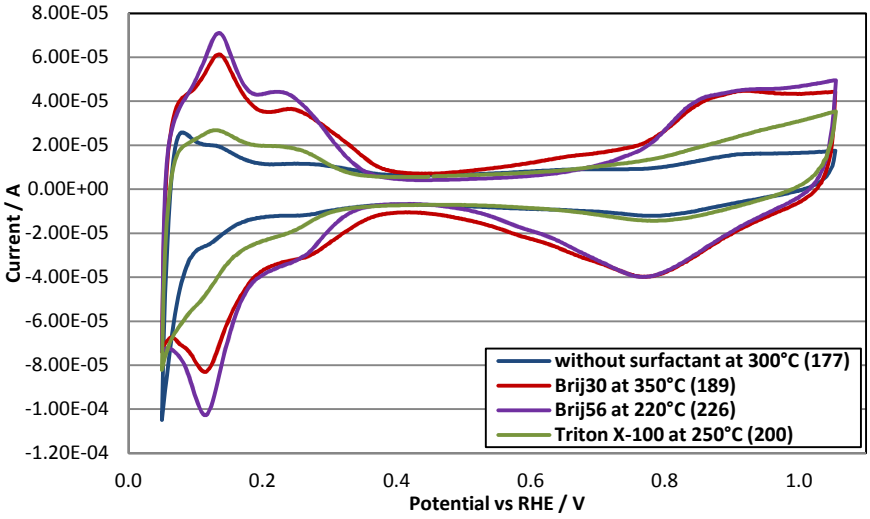

Figure 43: CVs of annealed samples with different surfactants (samples 177, 189, 226 and 200)

Table 29: ECSAs of annealed samples with different surfactants (samples 177, 189, 226 and 200)

	ECSA
	cm²/mg Pt
Without surfactant **(177)**	**59**
Brij30 **(189)**	**200**
Brij56 **(226)**	**190**
Triton X-100 **(200)**	**79**

These CV measurements show that the surfactants are capable of preventing the particles from agglomerating during the annealing step (see Figure 43 and Table 29). Sample 189 was tempered at a higher temperature than sample 177 and showed an

ECSA that is more than 3 times higher. Brij 56 also showed quite promising results while Triton X-100 seems to be not suitable.

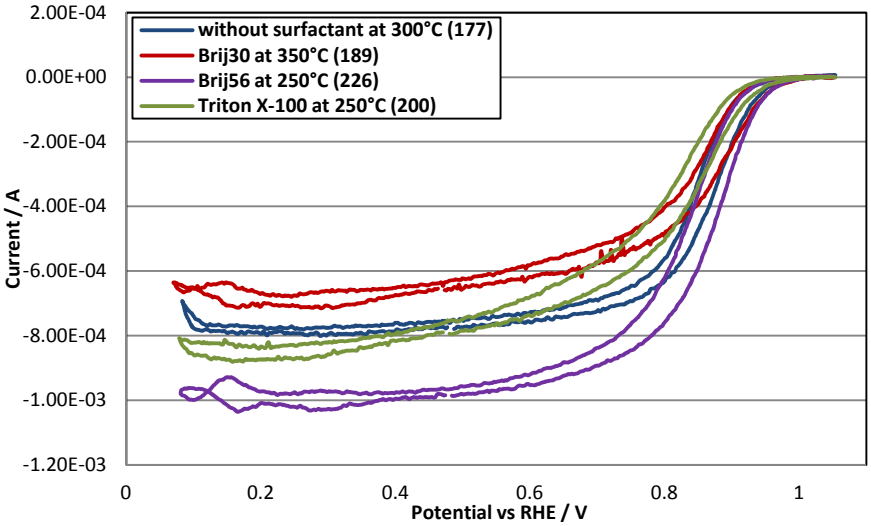

Figure 44: ORR of annealed samples with different surfactants (samples 177, 189, 226 and 200)

Table 30: ORR activity results of annealed samples with different surfactants (samples 177, 189, 226 and 200)

	Specific activity	Mass activity
	mA/cm²	**A/mg Pt**
Without surfactant **(177)**	**0.871**	**0.052**
Brij30 **(189)**	**0.294**	**0.059**
Brij56 **(226)**	**0.371**	**0.071**
Triton X-100 **(200)**	**0.369**	**0.029**

Because Brij30 and Brij56 yield similar ECSA results (see Table 29), Brij30 was the surfactant of choice due to its liquid state and the handling in the big scale manufacturing process. The ORR results are also quite promising in both cases but cannot be compared directly because the samples 189 and 226 were tempered at different temperatures (350 and 250°C).

To determine the optimal amount of surfactant 3 samples with different Brij-30 loadings were prepared (0.005, 0.01 and 0.02 equivalents, 1 equivalent equals the molar sum of platinum and cobalt). The samples were tempered at 350°C.

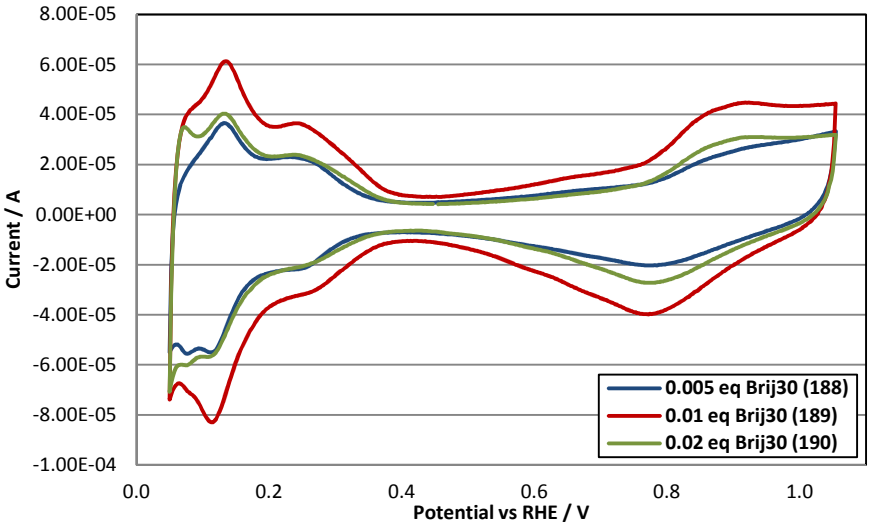

Figure 45: CVs of H_2SO_4 leached, with surfactant annealed catalysts (samples 188-190)

Table 31: ECSAs of H_2SO_4 leached, with surfactant annealed catalysts (samples 188-190)

	ECSA
	cm^2/mg Pt
0.005 eq Brij30 **(188)**	**106**
0.01 eq Brij30 **(189)**	**200**
0.02 eq Brij30 **(190)**	**122**

The ECSA results show that 0.01 equivalents seem to be optimal for the purpose of preventing agglomeration and not interfering with the nanoparticle formation (see Figure 45).

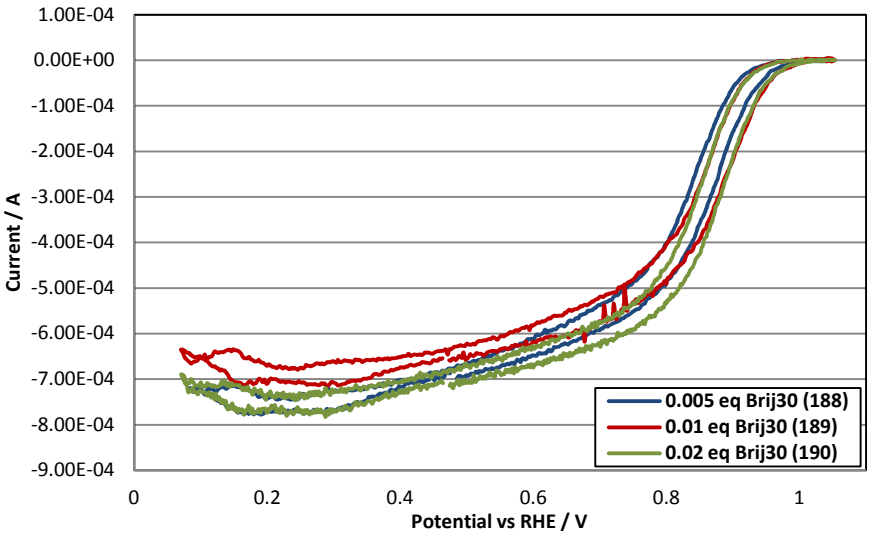

Figure 46: ORR of H_2SO_4 leached, with surfactant annealed samples (188-190)

Table 32: ORR activity results of H_2SO_4 leached, with surfactant annealed catalysts (samples 188-190)

	Specific activity	Mass activity
	mA/cm²	**A/mg Pt**
0.005 eq Brij30 **(188)**	**0.342**	**0.036**
0.01 eq Brij30 **(189)**	**0.294**	**0.059**
0.02 eq Brij30 **(190)**	**0.422**	**0.051**

The ORR results confirm our conclusion of the ECSA results (see Figure 46 and Table 32). For all further experiments 9 µl Brij30 were used for our GDE sheet of 2.2x2.2 cm². This amount shows optimal properties as stabilizer and has the beneficial property of ensuring better impregnation of the solution on our GDEs.

The surfactant was removed from our catalysts by the washing step in H_2O:IPA before all electrochemical measurements.

It is also observed that the active layer of the GDE degrades at temperatures above 350°C.

3.2.5.2 CV linear scan measurements

For these experiments catalysts with a Pt:Co ratio of 1:5 and 1:7 were prepared, leached with HCl and annealing steps at 180, 200, 220 and 240°C were conducted.

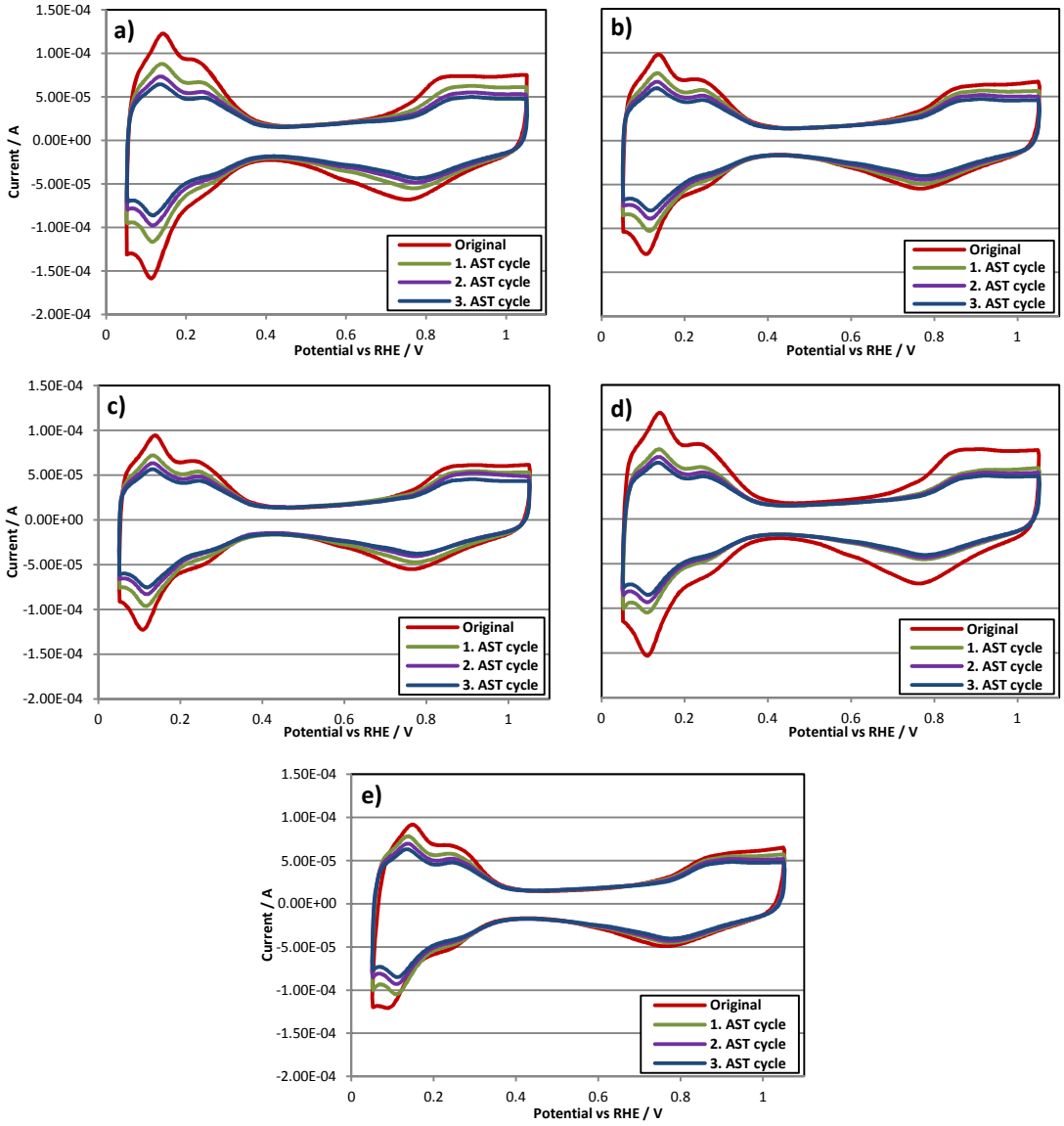

Figure 47: CVs of Pt:Co 1:5 catalysts before and after AST; a) non-stabilized sample (ÜKH41); b) stabilized by HCl leaching and annealing at 180°C (219); c) stabilized by HCl leaching and annealing at 200°C (218); d) stabilized by HCl leaching and annealing at 220°C (220); e) stabilized by HCl leaching and annealing at 240°C (221)

Table 33: ECSAs of acid leached and annealed catalysts before and after AST (samples 218-221)

	ÜKH41	219	218	220	221
	-	180°C	200°C	220°C	240°C
	cm²/mg Pt				
Original	**372**	**321**	**314**	**387**	**295**
555 AST cycles	**275**	**254**	**260**	**258**	**258**
1110 AST cycles	**227**	**217**	**237**	**238**	**238**
1665 AST cycles	**190**	**202**	**200**	**206**	**206**

Table 34: Relative ECSA loss during AST (samples 218-221)

	ÜKH41	219	218	220	221
	-	180°C	200°C	220°C	240°C
	Relative loss / %				
Original	-	-	-	-	-
555 AST cycles	**26**	**21**	**17**	**33**	**13**
1110 AST cycles	**39**	**32**	**24**	**38**	**19**
1665 AST cycles	**49**	**37**	**36**	**47**	**30**

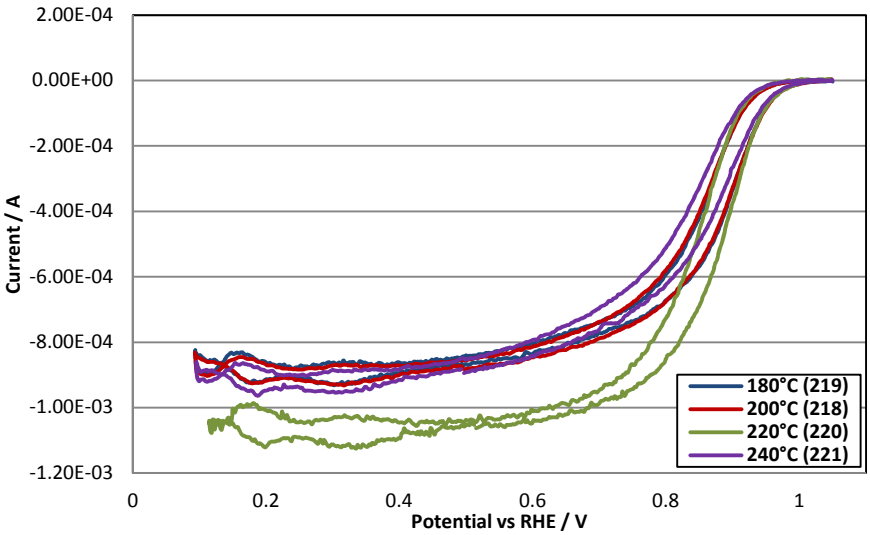

Figure 48: ORR of HCl leached, with surfactant annealed samples at various temperatures (samples 218-221)

Table 35: ORR activity results of HCl leached, with surfactant annealed samples at various temperatures (samples 218-221)

	Specific activity	Mass activity
	mA/cm²	A/mg Pt
180°C (219)	**0.366**	**0.091**
200°C (218)	**0.364**	**0.090**
220°C (220)	**0.452**	**0.112**
240°C (221)	**0.267**	**0.066**

For our catalysts with a Pt:Co ratio of 1:5 the annealing steps have a beneficial effect on stability as well as on the catalytic activity (see Figure 47 and Figure 48 as well as Table 33, Table 34 and Table 35). Based on the ORR results the annealing step is optimal at 220°C. If activity and stability are considered, the most favorable annealing temperature is between 200 and 220°C.

In this case all annealing steps were conducted in nitrogen atmosphere. Further progress could be achieved by tempering the catalysts in other atmospheres (e.g. carbon monoxide).

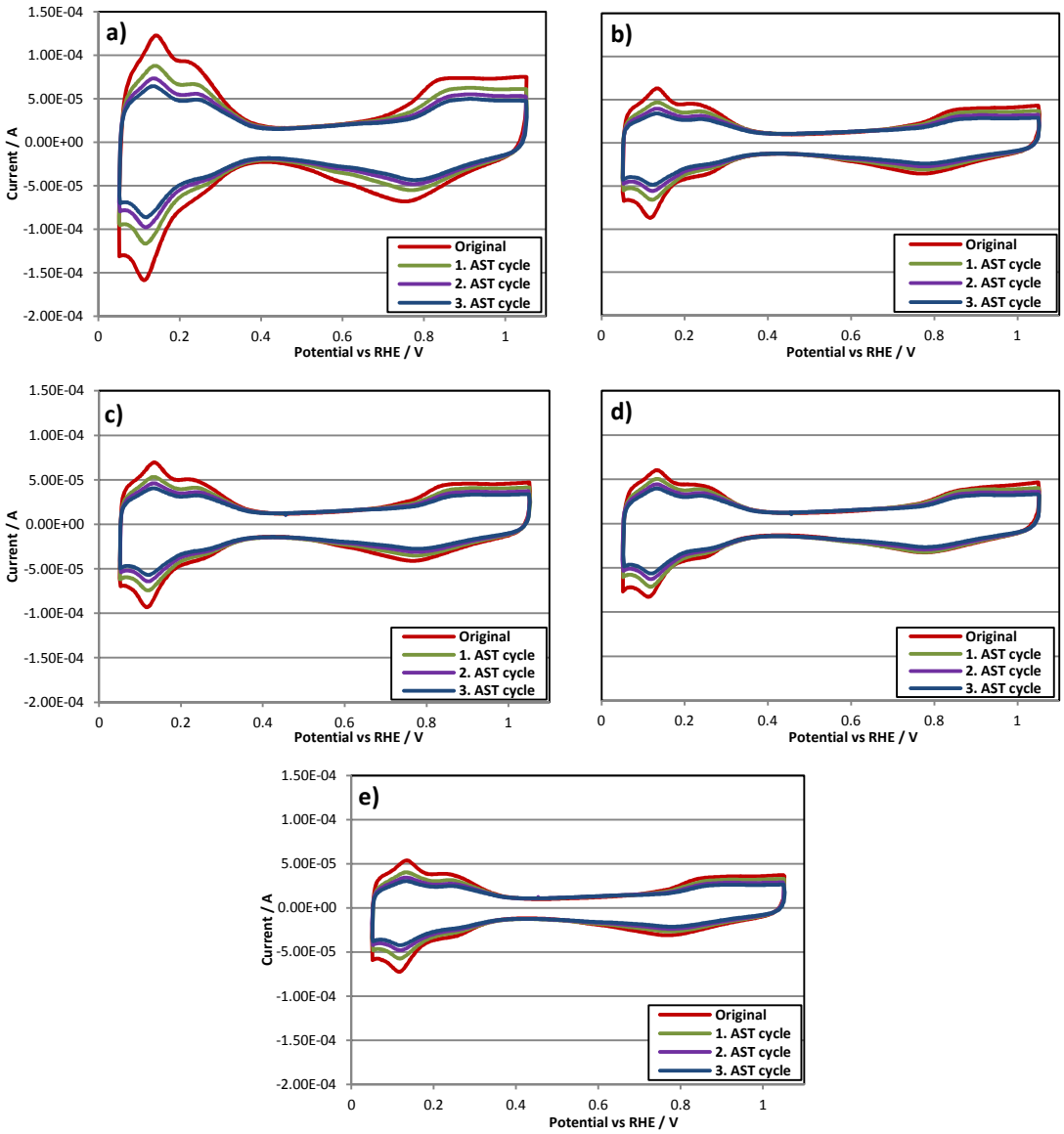

Figure 49: CVs of Pt:Co 1:7 catalysts before and after AST; a) non-stabilized sample (ÜKH41); b) stabilized by HCl leaching and annealing at 180°C (222); c) stabilized by HCl leaching and annealing at 200°C (223); d) stabilized by HCl leaching and annealing at 220°C (224); e) stabilized by HCl leaching and annealing at 240°C (225)

Table 36: ECSAs of acid leached and annealed catalysts before and after AST (samples ÜKH41, 222-225)

	ÜKH41	222	223	224	225
	-	180°C	200°C	220°C	240°C
			cm²/mg Pt		
Original	**372**	**198**	**223**	**189**	**178**
555 AST cycles	**275**	**158**	**165**	**151**	**131**
1110 AST cycles	**227**	**125**	**140**	**138**	**110**
1665 AST cycles	**190**	**118**	**118**	**119**	**91**

Table 37: Relative ECSA loss during ASTs (samples ÜKH41, 222-225)

	ÜKH41	222	223	224	225
	-	180°C	200°C	220°C	240°C
	Relative loss / %				
Original	-	-	-	-	-
555 AST cycles	**26**	**20**	**26**	**20**	**26**
1110 AST cycles	**39**	**37**	**37**	**27**	**38**
1665 AST cycles	**49**	**40**	**47**	**37**	**49**

All Pt:Co 1:7 catalysts have a smaller ECSA and are less stable than Pt:Co 1:5 samples.

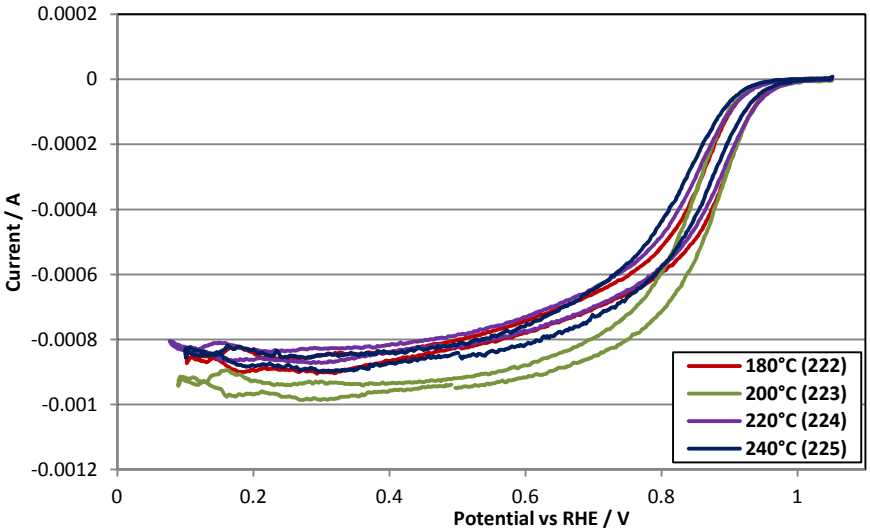

Figure 50: ORR of HCl leached, with surfactant annealed samples at various temperatures (samples 222-225)

Table 38: ORR activity results of HCl leached, with surfactant annealed samples at various temperatures (samples 218-221)

	Specific activity	Mass activity
	mA/cm²	A/mg Pt
180°C (222)	**0.271**	**0.067**
200°C (223)	**0.274**	**0.068**
220°C (224)	**0.229**	**0.057**
240°C (225)	**0.170**	**0.042**

The ORR measurements show similar results than the ECSA. All Pt:Co 1:7 samples have a smaller activity compared to Pt:Co 1:5 catalysts. Considering ECSA, stability and activity the ratio of platinum to cobalt of 1:5 is favorable.

3.2.5.3 TGA

For the big scale production process it would be beneficial if the surfactant can be detached thermally. To test the thermal removal, thermogravimetric analysis of catalyst samples with and without surfactants were conducted (results are shown in Figure 51).

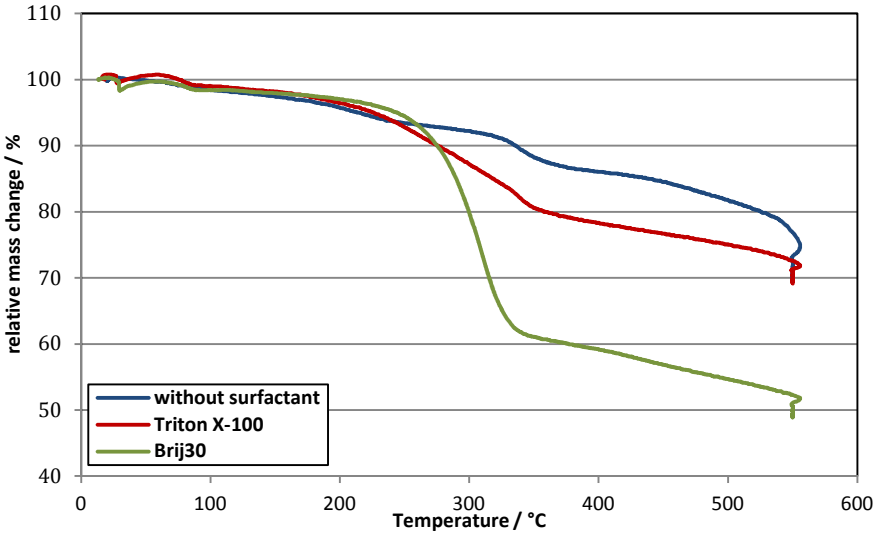

Figure 51: Results oft the thermogravimetric analysis

The results show that both surfactants can be removed by heating the GDE to around 340°C. Figure 51 shows that above this temperature all three curves are more or less parallel.

Unfortunately this temperature is not suitable for the production process with this active layer. As mentioned above the active layer degrades by temperatures around 350°C. Because both Brij surfactants showed quite promising properties the next obvious step is carrying on exploring the effect of smaller polyoxyethylene lauryl ether surfactants that can be removed at lower temperatures.

4 Summary and Outlook

The sample preparation was challenging because an impregnation solution premixed with a reducing agent is needed for a big scale manufacturing process. Therefore we investigated different agents to find one with optimal reducing properties. Too strong reducing agents reduce the precursor salts before impregnation and with too weak ones no reduction occurs at all. In principle the reduction has to be activated in a range of 100-300°C because temperatures up to 100° are needed to evaporate water and isopropanol of the impregnation solution and above 300°C the active layer of the GDE degrades. Furthermore the reaction products of the reducing agent should be easily removable. Ethylene glycol was found to meet all these criteria.

The optimal ratio of platinum and cobalt was determined by conducting experiments with various stoichiometric ratios of these metals. While optimizing the reducing parameters the ratios Pt:Co 1:5 and 1:7 gave most promising results. The preliminary findings showed that platinum is reduced first and activates the cobalt reduction

forming contrary core-shell-nanoparticles: Platinum core and cobalt shell. This finding is supported by the observations that cobalt cannot be reduced without any platinum (5 % platinum is sufficient) and that CV measurements in basic conditions show only a cobalt peak and no hydrogen adsorption peaks of platinum (see Figure 52).

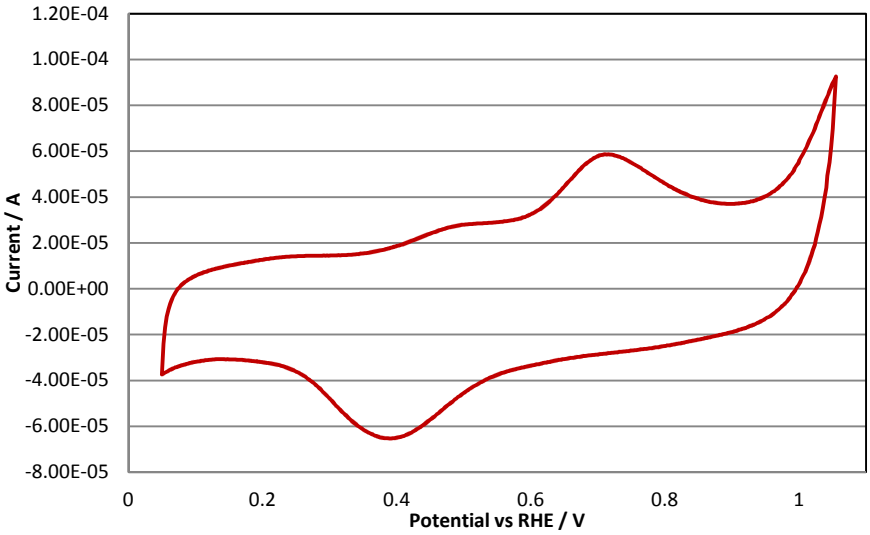

Figure 52: CV of Pt:Co 1:5 catalyst in a 0.1 M potassium hydroxide solution (sample 137)

Because of the formation of platinum core cobalt shell particles the cobalt layer is dissolved in acidic conditions and in the region of the platinum cobalt interface there seem to be a certain alloying content. This effect explains the activity enhancement compared to pure platinum. An increase of the alloying content may be achieved by annealing steps in carbon monoxide atmosphere. Because of the high affinity of carbon monoxide to platinum this annealing step enriches the platinum content on the surface [32]. This effect could also have a positive influence on the stability in acidic conditions.

By changing the reducing atmosphere from air to nitrogen the formation of cobalt oxide can be suppressed to a great extent. Therefore the reduction in nitrogen is more reliable. Considering the big scale process reliability is essential and most necessary.

The temperature of 240°C gives a good reaction rate and is optimal to form nanoparticles. By changing the temperature only small changes occur. For the manufacturing process we assume that the temperature profile has to be optimized again.

An acid leaching step in combination with an annealing step at 200° is the most promising stabilization procedure and sequence (see Figure 53). Samples 155-157 were prepared identically and only differ in the post reduction treatment. The ECSA of sample 155, that is a non-stabilized catalyst and acts as benchmark, decreased by 71 % after 1665 AST cycles. Sample 156, which was leached with 10%vol H_2SO_4 for 30

minutes, showed a significant increase of the ECSA as well as of the stability. Sample 157 was leached with H_2SO_4 and tempered at 200°C in a nitrogen atmosphere for 60 minutes. This stabilization sequence leads to a loss of ECSA of 31%.

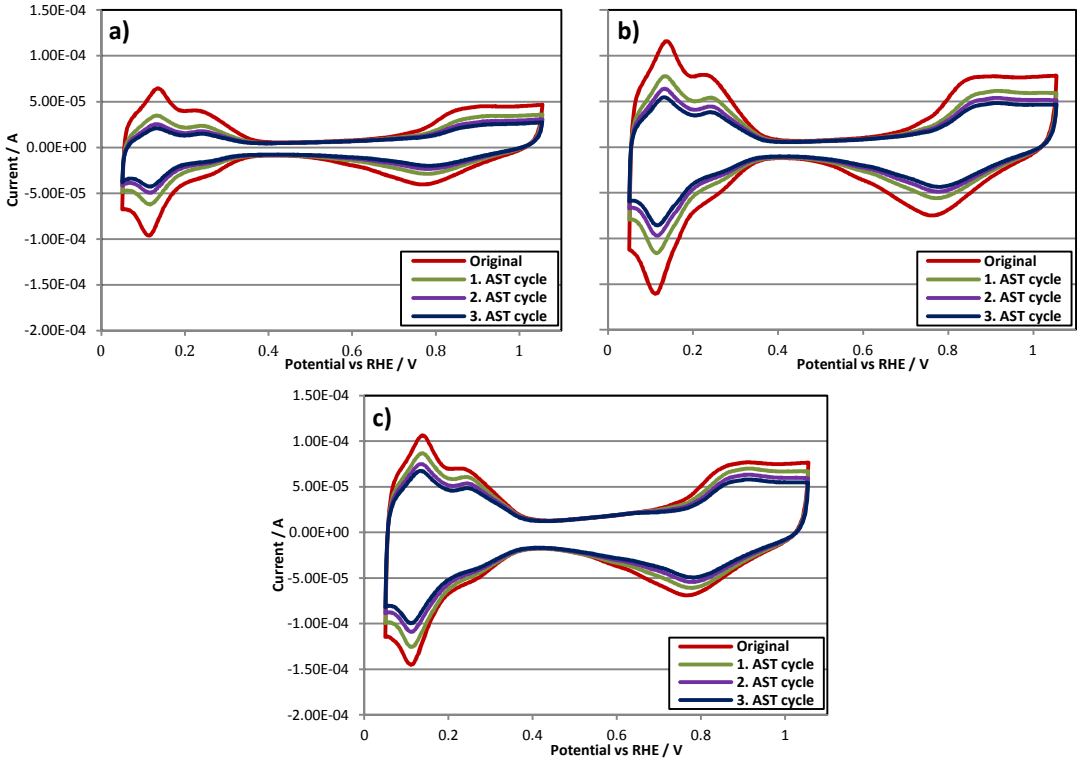

Figure 53: Staircase CVs of Pt:Co 1:5 catalysts before and after AST; a) non-stabilized sample (155); b) stabilized by H_2SO_4 leaching (159); c) stabilized by H_2SO_4 leaching and annealing at 200°C (157)

Table 39: ECSAs and relative loss of stabilized and non-stabilized samples before and after AST (155-157)

	155	155	156	156	157	157
	-	-	H_2SO_4	H_2SO_4	H_2SO_4 200°C	H_2SO_4 200°C
	cm²/mg Pt	**%**	**cm²/mg Pt**	**%**	**cm²/mg Pt**	**%**
Original	**191**	**-**	**380**	**-**	**337**	**-**
555 AST cycles	**93**	**51**	**234**	**38**	**302**	**11**
1110 AST cycles	**68**	**65**	**194**	**49**	**261**	**22**
1665 AST cycles	**55**	**71**	**174**	**54**	**234**	**31**

As can be seen from the data in Table 39 by this stabilization sequence the ECSA can be significantly increased while the relative loss of ECSA can be reduced by almost 60 %.

By deposition of an additional platinum layer in a second reduction step we observed an increase in stability of the catalyst samples. Because the stabilization is not as good as the case described above and a second step is unpractical for the manufacturing process this strategy has not been further investigated.

To prevent the nanoparticles from agglomeration during the annealing steps various surfactants were added. The polyoxyethylene lauryl ether Brij30 was the surfactant of choice due to its liquid state and the handling in the manufacturing process. Apart from these advantages this surfactant has the beneficial side effect that the solution impregnates much better into the GDE sheet. After drying the sheet at 100°C the impregnation solution without surfactant consists only of precursor salts and ethylene glycol. The surfactant acts as an intermediary phase between EG and the hydrophobic active layer.

5 Literature

[1] R. Bashyam, P. Zelenay, Nature 443 (2006) 63.

[2] J. Zhang, Z. Xie, J. Zhang, Y. Tang, C. Song, T. Navessin, Z. Shi, D. Song, H. Wang, D.P. Wilkinson, Z.-S. Liu, S. Holdcroft, Journal of Power Sources 160 (2006) 872.

[3] Y. Wang, K.S. Chen, J. Mishler, S.C. Cho, X.C. Adroher, Applied Energy 88 (2011) 981.

[4] B. Fang, B.N. Wanjala, J. Yin, R. Loukrakpam, J. Luo, X. Hu, J. Last, C.-J. Zhong, International Journal of Hydrogen Energy 37 (2012) 4627.

[5] Q. Li, R. He, J.O. Jensen, N.J. Bjerrum, Chemistry of Materials 15 (2003) 4896.

[6] V. Hacker, S. Mitsushima, in:, Advanced Studies of Polymer Electrolyte Fuel Cells - 5th International Summer School, 2012, pp. 20–24.

[7] V. Hacker, E. Wallnöfer-Ogris, in:, Advanced Studies of Polymer Electrolyte Fuel Cells - 4th International Summer School, 2011, pp. 11–15.

[8] C. Yang, P. Costamagna, S. Srinivasan, J. Benziger, a. B. Bocarsly, Journal of Power Sources 103 (2001) 1.

[9] Q. Li, R. He, J.-A. Gao, J.O. Jensen, N.J. Bjerrum, Journal of The Electrochemical Society 150 (2003) A1599.

[10] M.S. Wilson, Journal of The Electrochemical Society 140 (1993) 2872.

[11] K. Kinoshita, Journal of The Electrochemical Society 137 (1990) 845.

[12] M. Nesselberger, S. Ashton, J.C. Meier, I. Katsounaros, K.J.J. Mayrhofer, M. Arenz, Journal of the American Chemical Society 133 (2011) 17428.

[13] V.R.P. Markovic, NM; Schmidt, TJ; Stamenkovic, Fuel Cells 1 (2001) 105.

[14] H. a. Gasteiger, S.S. Kocha, B. Sompalli, F.T. Wagner, Applied Catalysis B: Environmental 56 (2005) 9.

[15] J.R.C. Salgado, E. Antolini, E.R. Gonzalez, Journal of The Electrochemical Society 151 (2004) A2143.

[16] K. Jayasayee, J. a. R. Van Veen, T.G. Manivasagam, S. Celebi, E.J.M. Hensen, F. a. de Bruijn, Applied Catalysis B: Environmental 111-112 (2012) 515.

[17] K.J.J. Mayrhofer, D. Strmcnik, B.B. Blizanac, V. Stamenkovic, M. Arenz, N.M. Markovic, Electrochimica Acta 53 (2008) 3181.

[18] E. Antolini, J. Salgado, M. Giz, E. Gonzalez, International Journal of Hydrogen Energy 30 (2005) 1213.

[19] P. Vanyek, in:, Handbook of Chemistry and Physics, 2004, pp. 8.21–8.31.

[20] G. Squadrito, in:, Advanced Studies of Polymer Electrolyte Fuel Cells - 4th International Summer School, 2011, pp. 53–56.

[21] David Thompsett, in:, Proton Exchange Membrane Fuel Cells, 2010, pp. 1–60.

[22] V.R. Stamenkovic, B.S. Mun, M. Arenz, K.J.J. Mayrhofer, C. a Lucas, G. Wang, P.N. Ross, N.M. Markovic, Nature Materials 6 (2007) 241.

[23] V. Stamenkovic, T. Schmidt, The Journal of Physical Chemistry B 106 (2002) 11970.

[24] M.T. Paffett, Journal of The Electrochemical Society 135 (1988) 1431.

[25] S. Chen, W. Sheng, N. Yabuuchi, P.J. Ferreira, L.F. Allard, Y. Shao-horn, Journal of Physical Chemistry C 113 (2009) 1109.

[26] V. Stamenkovic, B.S. Mun, K.J.J. Mayrhofer, P.N. Ross, N.M. Markovic, J. Rossmeisl, J. Greeley, J.K. Nørskov, Angewandte Chemie 118 (2006) 2963.

[27] F. Lai, L. Sarma, H. Chou, The Journal of Physical Chemistry C 113 (2009) 12674.

[28] Z. Yu, J. Zhang, Z. Liu, J.M. Ziegelbauer, H.L. Xin, I. Dutta, D. Muller, F.T. Wagner, The Journal of Physical Chemistry C (2012) 120822193642009.

[29] C.H. Hamann, V. Wolf, Elektrochemie, 2005.

[30] A. Rodes, M.A. Zamakhchari, K. El Achi, J. Clavilier, Journal of Electroanalytical Chemistry 305 (1991) 115.

[31] S. Mitsushima, in:, Advanced Studies of Polymer Electrolyte Fuel Cells - 4th International Summer School, 2011, pp. 57–64.

[32] E.G. Ciapina, E. a. Ticianelli, Electrochimica Acta 58 (2011) 172.

6 Appendix

6.1 Abbreviations and Acronyms

AST	Accelerated stress test
CV	Cyclic voltammetry
ECSA	Electrochemical active surface area
EG	Ethylene glycol
FC	Fuel Cell
GDE	Gas diffusion electrode
HHV	Higher heating value
HOR	Hydrogen Oxidation Reaction
HT	High Temperature
IPA	Isopropyl alcohol

LHV	Lower heating value
LT	Low Temperature
ORR	Oxygen Reduction Reaction
PBI	polybenzimidazole
PEM	Polymer Electrolyte Membrane
PFSA	perfluorosulfonic acid
RDE	Rotating disk electrode
RF	Roughness factor
TEM	Transmission Electron Microscope
TGA	Thermo gravimetric analysis

6.2 Supplementary Information

In this section all sample preparation details are described. All chemicals are commercially available and were used as received. Ultrapure water was used for all solutions, samples and for the electrolyte.

Procedure

The given amount of solution was displaced on a GDE sheet of 2.2x2.2 cm² at 100°C. The GDE sheet was dried for 30 minutes at this temperature. The GDE sheets were instantly placed on a metal plate and put in the oven. After 10 minutes of reduction time the samples were removed from the oven, cooled to room temperature and washed in a mixture of IPA and water. In the case of stabilization procedures the details are given in section 2.1.1.

After preparing the catalyst for electrochemical measurements (see section 2.1.2) the following procedures were applied:

- Starting cycles (in nitrogen saturated electrolyte)
  - Start/stop potential 0.455 V
  - Upper vertex 1.055 V
  - Lower vertex 0.050 V
  - Scan rate 0.100 V/s
  - Cycles 5
- Cleaning cycles (in nitrogen saturated electrolyte)
  - Start/stop potential 0.455 V
  - Upper vertex 1.200 V
  - Lower vertex 0.050 V

    - Scan rate 0.500 V/s
    - Cycles 200
- Measurement ECSA (in nitrogen saturated electrolyte)
    - Start/stop potential 0.455 V
    - Upper vertex 1.055 V
    - Lower vertex 0.050 V
    - Scan rate 0.050 V/s
    - Cycles 3
- Measurement ORR (in oxygen saturated electrolyte, rotating disk at 1600 rpm)
    - Start/stop potential 0.455 V
    - Upper vertex 1.055 V
    - Lower vertex 0.050 V
    - Scan rate 0.050 V/s
    - Cycles 5
- Measurement stabilization (in nitrogen saturated electrolyte)
    - AST cycles (see section 2.2.1.2)
    - Measurement ECSA (see above)
    - repetition 3

Table 40: List of impregnation solutions

Solution	Pt:Co	H_2O	IPA	EG	Pt^{4+}	Co^{2+}
number	**ratio**	**ml**	**ml**	**ml**	**mg/ml**	**mg/ml**
4	3:1	0.596	1.096	0.249	38.31	3.86
6	1:3	0.810	0.810	0.279	19.36	17.76
7	1:5	0.570	0.570	0.750	19.46	29.59
10	Pt	0.447	0.447	0.056	19.36	-
11	Pt	0.400	0.400	0.100	1.94	-
15*	1:5	-	0.475	-	19.56	23.41
18**	1:20	-	0.450	-	4.80	29.00
20	1:1	0.867	0.867	0.166	19.36	5.85
21	1:7	0.700	0.700	0.499	19.36	40.94
25	1:1	0.575	0.575	0.750	19.36	5.85
26	1:3	0.575	0.575	0.750	19.36	17.54
27	1:7	0.575	0.575	0.750	19.36	40.94
28	1:10	0.575	0.575	0.750	19.36	58.48
30	1:5	1.886	1.886	0.971	19.36	29.24
31	1:5	0.732	0.732	0.377	19.36	29.24

* solution for samples with formic acid as reducing agent

** solution for samples with formaldehyde as reducing agent (0.55 ml 30 % formaldehyde solution)

Table 41: List of samples

Sample	Pt:Co	Solution	Volume	Pt	Co	Temp.
number	**ratio**	**number**	**ml**	**mg/cm²**	**mg/cm²**	**°C**
148*	1:5	**15**	0.20	0.81	0.97	100
149*	1:20	**18**	0.20	0.20	1.20	150
	Pt	**10**	0.20	0.80	-	240
153*	1:5	**7**	0.30	1.21	1.83	240
154*	1:5	**7**	0.30	1.21	1.83	240
155	1:5	**7**	0.30	1.21	1.83	250
156	1:5	**7**	0.30	1.21	1.83	250
157	1:5	**7**	0.30	1.21	1.83	250
158	1:1	**20**	0.30	1.20	0.60	240
159	1:3	**6**	0.30	1.20	1.10	240
160	1:7	**21**	0.30	1.20	4.17	240
161*	1:10	**28**	0.15	0.60	2.98	240
162	1:5	**7**	0.15	0.60	0.92	240
	1:3	**6**	0.15	0.60	0.55	240
163	1:5	**7**	0.15	0.60	0.92	240
	1:3	**6**	0.15	0.60	0.55	240
164	1:5	**7**	0.15	0.60	0.92	240
	1:3	**6**	0.15	0.60	0.55	240
165	1:5	**7**	0.25	1.01	1.53	240
	Pt	**11**	0.300	0.12	-	200
173	1:5	**30**	0.25	1.00	1.51	230
174	1:5	**30**	0.25	1.00	1.51	230
175	1:5	**31**	0.25	1.00	1.51	230
176	1:5	**30**	0.25	1.00	1.51	230
177	1:5	**30**	0.25	1.00	1.51	230
188	1:5	**7**	0.25	1.01	1.53	220
189	1:5	**7**	0.25	1.01	1.53	220
190	1:5	**7**	0.25	1.01	1.53	220
200	1:5	**7**	0.25	1.01	1.53	220
201	1:1	**25**	0.28	1.12	0.34	230
202	1:3	**26**	0.25	1.00	0.91	230
203	1:5	**7**	0.25	1.01	1.53	230
204	1:7	**27**	0.25	1.00	2.11	230
205	1:5	**7**	0.25	1.01	1.53	220
206	1:5	**7**	0.25	1.01	1.53	230

Sample	Pt:Co	Solution	Volume	Pt	Co	Temp.
number	**ratio**	**number**	**ml**	**mg/cm²**	**mg/cm²**	**°C**
207	1:5	**7**	0.25	1.01	1.53	240
208	1:5	**7**	0.25	1.01	1.53	250
209*	1:5	**7**	0.25	1.01	1.53	240
211	1:5	**7**	0.25	1.01	1.53	240
212	1:5	**7**	0.25	1.01	1.53	240
213	1:5	**7**	0.25	1.01	1.53	240
214	1:5	**7**	0.25	1.01	1.53	240
215	1:5	**7**	0.25	1.01	1.53	240
216	1:5	**7**	0.25	1.01	1.53	240
	Pt	**10**	0.05	0.20	-	240
217	1:5	**7**	0.25	1.01	1.53	240
	3:1	**4**	0.25	0.20	0.02	240
218	1:5	**7**	0.25	1.01	1.53	240
219	1:5	**7**	0.25	1.01	1.53	240
220	1:5	**7**	0.25	1.01	1.53	240
221	1:5	**7**	0.25	1.01	1.53	240
222	1:7	**27**	0.25	1.00	2.11	240
223	1:7	**27**	0.25	1.00	2.11	240
224	1:7	**27**	0.25	1.00	2.11	240
225	1:7	**27**	0.25	1.00	2.11	240
229	1:5	**7**	0.25	1.01	1.53	240

* reduction in air

6.3 List of figures

6.4 List of tables